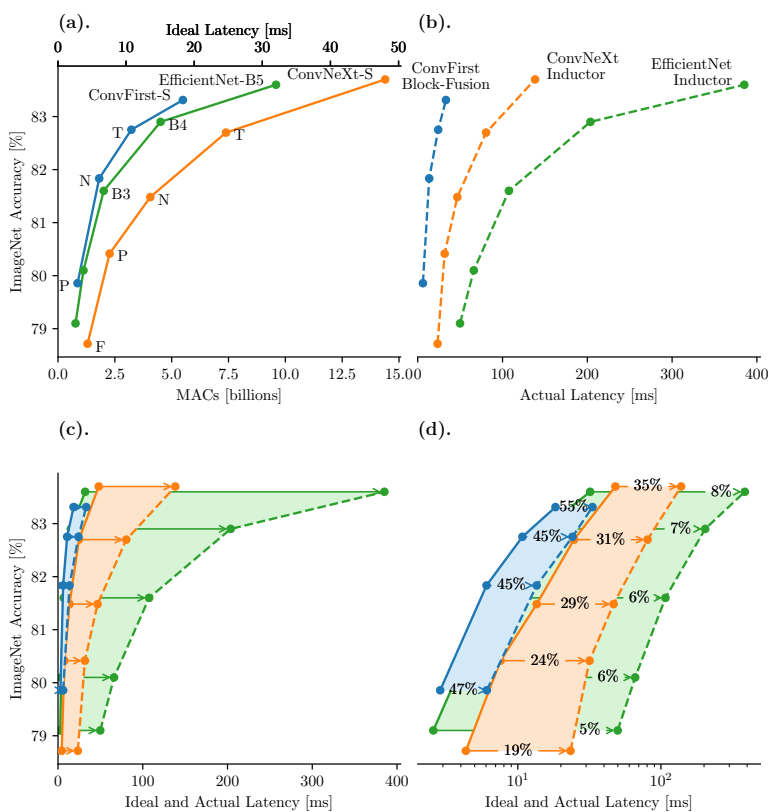


On the Efficiency of Convolutional Neural Networks

Andrew Lavin

May 21, 2024



Efficiency gap plots compare ideal and actual latency and quantify the difference as computational efficiency. **(a)**. Dividing arithmetic complexity (MACs) by peak arithmetic throughput yields the *ideal latency*. **(b)**. Inference time on the GPU is the *actual latency*. **(c)**. The ideal latency of ConvNeXt is longer than the actual latency of ConvFirst. **(d)**. Low computational efficiency causes a wide gap between ideal and actual latency. EfficientNet ranges from 5% – 8% and has a wide gap. Our ConvFirst model with block-fusion kernels ranges from 47% – 55% and has a narrow gap. We used an NVIDIA A5000 GPU with float16 and batch size 128.

Abstract

Since the breakthrough performance of AlexNet in 2012, convolutional neural networks (convnets) have grown into extremely powerful vision models. Deep learning researchers have used convnets to perform vision tasks with accuracy that was unachievable a decade ago. Yet computer scientists make computational efficiency their primary objective. They seek algorithms that use the fewest operations and the least communication. Confronted with the immense computation that convnets use, deep learning researchers also became interested in efficiency. They replaced expensive conv2d layers with sequences of degenerate layers that have less arithmetic complexity. They used network architecture search to find the model hyperparameters that yield the greatest accuracy with the fewest operations. However, the engineers who deployed these efficient convnets soon realized that they were slower than the previous generation, despite using fewer operations. Many reverted to older models that ran faster. Hence researchers switched the objective of their search from arithmetic complexity to latency and produced a new wave of models that performed better. Paradoxically, these models also used more operations. Skepticism grew among researchers and engineers alike about the relevance of arithmetic complexity.

Contrary to the prevailing view that latency and arithmetic complexity are irreconcilable, a simple formula relates both through computational efficiency. This insight enabled us to co-optimize the separate factors that determine latency. We observed that the degenerate conv2d layers that produce the best accuracy-complexity trade-off also use significant memory resources and have low computational efficiency. We devised *block fusion* algorithms to implement all the layers of a residual block in a single kernel, thereby creating temporal locality, avoiding communication, and reducing workspace size. Our ConvFirst model with block-fusion kernels has less arithmetic complexity and greater computational efficiency than baseline models and kernels. ConvFirst ran approximately four times as fast as ConvNeXt at equal accuracy on the ImageNet-1K classification task.

On the journey to this result, we created novel tools. We made the *efficiency gap* plot to show accuracy, arithmetic complexity, latency, and computational efficiency on the same axes. The plot illustrates how computational efficiency distorts model efficiency to produce latency. We created *waterline analysis* to extend roofline analysis to a sequence of parallel kernels. We devised the *tensor machine*, a simple abstract computer for tensor programs, and used it to plan block-fusion kernels. Our unified approach to convnet efficiency envisions a new era of models and kernels that achieve greater accuracy at lower cost.

Contents

1	Introduction	2
2	Related Work	3
3	Efficiency Gap: How Computational Efficiency Distorts Model Efficiency	5
3.1	Measuring Efficiency	6
3.2	Visualizing Efficiency	8
4	Waterline: A Simple Performance Model for a Sequence of Parallel Kernels	11
4.1	Waterline Analysis of Conv2d Layers	12
4.1.1	Conv2d and its Degenerate Cases	12
4.1.2	Operational Intensity of Conv2d	14
4.1.3	Degenerate Conv2d and the op:byte Waterline	17
4.2	Waterline Analysis of Convnet Models	19
4.3	Mediant Operational Intensity	20
5	Block Fusion: An Optimization for Degenerate Conv2d Layers	23
5.1	Tensor Machines	23
5.2	Feed-Forward Network	25
5.3	ConvFirst Block	26
5.3.1	Block-Fusion Kernel for ConvFirst	28
5.3.2	Waterline Analysis of ConvFirst	30
5.4	MBConv Block	30
5.4.1	Block-Fusion Kernel for MBConv	32
5.4.2	Waterline Analysis of MBConv	36
5.5	CUDA Kernels	36
5.5.1	ConvFirst CUDA Kernel	37
5.5.2	MBConv CUDA Kernel	39
5.5.3	Kernel Benchmarks	40
5.6	Depth-First Execution	44
6	ConvFirstNet: Striving for Computational Efficiency and Model Efficiency	44
6.1	The Design of ConvFirstNet	45
6.2	Waterline Analysis of ConvFirstNet	46

6.3	ConvFirstNet Model Experiments	49
6.4	Results	49
7	Conclusion	52
A	ConvFirstNet Speed Projections	59
B	Amdahl's Roofline	65

1. Introduction

The conv2d layer is the basic building block of convolutional neural networks (convnets). It accounts for most of a convnet's computation, so naturally it has been the focus of efforts to make convnets more efficient. On the one hand, computer scientists improved the computational efficiency of the conv2d layer by examining its arithmetic complexity and data movement and applying this understanding to create more efficient algorithms and hardware. On the other hand, deep learning researchers reduced the arithmetic complexity of the traditional conv2d layer by factoring it into a sequence of degenerate layers that perform fewer total operations.

Computer scientists improved the speed of first-wave convnets, while deep learning researchers created a second wave that used fewer operations to achieve the same accuracy. In other words, the original convnets benefited from improved *computational efficiency* while the new ones had greater *model efficiency*. In practice, the second-wave models suffered from significantly worse computational efficiency that undermined their superior model efficiency.

Deep learning researchers responded in different ways to the efficiency paradox posed by the second wave. Some employed network architecture search and found the convnet models with the lowest latency on one or more software and hardware platforms. Others exploited correlations between model hyperparameters and computational efficiency and discovered that convnets could be made faster simply by making them wider (i.e., increasing the number of channels in every layer). Some optimized hardware architecture and memory placement algorithms to make new processors that ran existing software more efficiently.

The result of these efforts was a third wave of convnets and accelerators that were suboptimal in various ways. Despite their improved computational efficiency, third-wave convnets often had worse model efficiency than second-wave convnets. Third-wave

accelerators performed with greater computational efficiency on all models, while devoting much larger die area to on-chip memory (SRAM). These accelerators had less peak arithmetic throughput per square millimeter than ones that used less SRAM, effectively increasing the cost of an arithmetic operation.

We take a new approach that elevates the importance of computation. We find the simple formula that relates model efficiency, computational efficiency, and latency, and plot all of these quantities on the same axes, thereby revealing the efficiency gap that explains the convnet efficiency problem. We extend roofline analysis to calculate the attainable latency of a sequence of parallel kernels; and we develop simple plots that reveal the latency and operational intensity of individual layers. We use a simple abstract tensor machine to express new algorithms and use it to design memory-efficient block-fusion kernels that greatly increase the attainable efficiency. We contribute a new convnet that is co-optimized for model efficiency and computational efficiency, train it, and benchmark it with CUDA kernels that implement our block-fusion algorithms. The results show greater model efficiency than our second-wave baseline and greater computational efficiency than the third-wave baseline. The combination of efficient model and kernels yields significantly lower latency at equal levels of accuracy.

We hope our approach contributes to a new wave of convnets, software, and hardware that achieves significantly greater efficiency.

2. Related Work

AlexNet [37] began the modern era of convnets with its breakthrough performance on the ImageNet [13] image classification benchmark. Since then, researchers have published a series of innovative models, introducing new layers that improved model efficiency. Network-in-Network used point-wise (1×1) convolutions [44]. ResNet contributed the residual block and bottleneck block, enabling deeper models and reducing the number of operations per activation [24]. Squeeze & Excitation networks introduced a lightweight, channel-wise attention mechanism that increased accuracy while adding few additional operations [28]. MobileNetV2 introduced the inverted residual block with depth-wise convolutions and a memory-efficient algorithm for computing it [59]. EfficientNet combined all of these ideas into a scalable model that shattered the state-of-the-art for model efficiency over a wide range of scales [63].

Early convnets used conv2d layers with 3×3 kernels or larger [42, 37, 60, 61, ...], and early works on computational efficiency focused on these layers. A straightforward

implementation achieved 96% computational efficiency on an NVIDIA GPU, because of the layer’s large operational intensity [39]. Subsequent works focused on fast algorithms that reduced the arithmetic complexity of the convnet block [47, 68, 8], culminating in GPU kernels exceeding 100% effective computational efficiency [41].

Recent convnets used point-wise [44] and depth-wise [7, 27] convolutions. These degenerate conv2d layers have less arithmetic complexity and increased model efficiency. Simultaneously, deep learning accelerators began to use matrix multiply accelerators that dramatically increased the peak arithmetic throughput [32, 53]. Decreasing operational intensity of the layers and increasing op:byte ratio of the accelerators put tremendous pressure on the software that runs the convnets. The result was that EfficientNet [63] had poor computational efficiency on a contemporary GPU using the best available software.

Several papers improved the performance of modern convnets by using inference latency as the model cost instead of arithmetic complexity [65, 26, 14, 6, 64, ...]. These papers measured latency using popular deep learning frameworks and inference engines without modification.

Yang et al. optimized the data-flow, blocking, and memory hierarchy of convnet accelerator hardware [74]. Zhang et al. co-optimized the size of matrix multiply accelerators, on-chip memory capacity, and the memory placement of weights and activations tensors [75]. Both these works assumed layer-by-layer execution, and both increased the on-chip memory capacity to avoid storing activations to DRAM between layers.

Radosavovic et al. [56] observed that the number of activations correlates with inference latency and searched for models with fewer activations. Dollar et al. [14] used a scaling rule that creates wider models, motivated by the observations that wider models have more operations per activation and hence greater computational efficiency.

Other works computed a small number of tiles in one layer before computing the next layer’s tiles that depend on them [1, 19]. This strategy created a depth-first execution of the convnet that reduced the size of the workspace needed to hold activations, making it possible to keep activations in a small on-chip memory. Depth-first execution has long been used to exploit spatial locality in image processing [57] and stencil programs [17]. It cannot traverse a layer that performs a global spatial reduction, such as Squeeze & Excitation [28]; nor does it exploit the channels dimension of a convnet. Depth-first execution complements our block-fusion strategy (see Section 5).

PyTorch 2 added the TorchInductor compiler backend that performs trivial layer fusions and accelerates inference [3]. We used TorchInductor as our baseline inference

engine.

Our recent work [40, 38] developed GPU kernels that compute all the layers of the FusedMBConv [21] or MBConv [59, 63] block in a single kernel. These block-fusion kernels exploit temporal locality to reduce workspace size and avoid DRAM memory transfers. This paper extends those results.

Following the success of the transformer architecture for sequence modeling [69], several works produced vision transformers [15, 10, 45, 67, 11, ...]. Vision transformers were scaled to very large models with high accuracy. Smith et al. [62] found that convnets scale as well as vision transformers with a similar training budget. The focus of this paper is convnets, but the methodology we developed applies equally well to transformers and convnet-transformer hybrids.

3. Efficiency Gap: How Computational Efficiency Distorts Model Efficiency

In physical science a first essential step in the direction of learning any subject is to find principles of numerical reckoning and methods for practicably measuring some quality connected with it. I often say that when you can measure what you are speaking about and express it in numbers you know something about it; but when you cannot measure it, when you cannot express it in numbers, your knowledge is of a meagre and unsatisfactory kind: it may be the beginning of knowledge, but you have scarcely, in your thoughts, advanced to the stage of *science*, whatever the matter may be.

William Thomson, 1st Baron Kelvin, 1883 [34]

In order to understand efficiency, we must first learn how to measure it. In this section we define various measures of efficiency. Some will already be known to the reader, others are borrowed from the field of high-performance computing, and one is novel. Where often-used metrics were not precisely named in previous literature, our nomenclature makes deliberate and unambiguous choices. Together our metrics describe the relationship between model and algorithm and illustrate how each contributes to performance.

After we have measured the different kinds of efficiency, we will develop a new kind of plot to visualize their relationships.

3.1. Measuring Efficiency

Model efficiency $\mathcal{E}_m(n)$ measures accuracy as a function of the number of mathematical operations n the model performs. This metric expresses the trade-off between the quality of the result (the accuracy) and the quantity of work (computation). Thus it measures the efficiency with which the model achieves the desired result. The accuracy of a model should increase as it scales to a larger number of operations, so we assume that the model efficiency function is monotonically increasing.

Model efficiency is not bounded by the physics of computation. It says nothing about the rate at which computation can be performed, so it cannot predict latency.

There is no theory of machine learning that predicts the accuracy of a trained model. Thus model efficiency is, for now, a purely empirical quantity. One measures model efficiency by instantiating a family of models at different scales (n), training each model instance on the desired task, and measuring the achieved accuracy.

Peak arithmetic throughput \mathcal{R}_i measures the fastest rate at which a processor can perform computation. It represents the *ideal* arithmetic throughput. Hardware manufacturers report peak arithmetic throughput in units of operations per second (OP/s or OPS). The unit TOPS indicates one trillion (10^{12}) operations per second. One multiply and add (i.e., one multiply-accumulate or MAC) is considered to be 2 OPs. Almost all of the computation performed by neural networks is multiply-add operations, so this definition of peak arithmetic throughput is useful for understanding ideal performance.

Ideal latency

$$(1) \quad t_i(n) = \frac{n}{\mathcal{R}_i}$$

is the fastest possible response time any model with n operations could theoretically achieve on a processor with peak arithmetic throughput \mathcal{R}_i .

Ideal efficiency

$$(2) \quad \mathcal{E}_i\left(\frac{n}{\mathcal{R}_i}\right) = \mathcal{E}_m(n)$$

is the greatest possible accuracy a model can achieve for a given latency.

Actual arithmetic throughput

$$(3) \quad \mathcal{R}_a(n) = \frac{n}{t_a(n)}$$

is the rate at which the processor and software perform the model's operations, where $t_a(n)$ is the *actual latency* measured for the model with n operations. Achieving high arithmetic throughput is a physics problem, bounded by the physical behavior of the processor's arithmetic units, memory systems, and the wires that connect them, and optimized by the algorithm that schedules the utilization of these resources. In principle one could better organize the processor and algorithm to achieve greater arithmetic throughput for a given model.

Actual efficiency

$$(4) \quad \mathcal{E}_a\left(\frac{n}{\mathcal{R}_a(n)}\right) = \mathcal{E}_m(n)$$

is the accuracy that the model, processor, and software achieve for a given latency.

Combining Equations (2) and (4),

$$(5) \quad \mathcal{E}_m(n) = \mathcal{E}_i\left(\frac{n}{\mathcal{R}_i}\right) = \mathcal{E}_a\left(\frac{n}{\mathcal{R}_a(n)}\right)$$

we observe that ideal and actual efficiency are both horizontal dilations of the model efficiency function.

Alternatively, we can write

$$(6) \quad \mathcal{E}_i(t) = \mathcal{E}_a\left(\frac{t}{\mathcal{C}}\right)$$

where

$$(7) \quad \mathcal{C}(n) = \frac{\mathcal{R}_a(n)}{\mathcal{R}_i}$$

is *computational efficiency*, the ratio of actual to peak arithmetic throughput. Thus computational efficiency expands the ideal efficiency function to produce actual efficiency.

We can also write the relationship in terms of latencies as

$$(8) \quad t_a(n) = \frac{t_i(n)}{\mathcal{C}(n)}$$

Using logarithmic scale we get

$$(9) \quad \log(t_a(n)) = \log(t_i(n)) - \log(\mathcal{C}(n))$$

so that $-\log(\mathcal{C}(n))$ is the amount by which the logarithm of the latency is increased because of imperfect computational efficiency. In an accuracy versus latency plot using logarithmic scale on the x-axis, the actual efficiency function is produced by shifting the ideal efficiency function by $-\log(\mathcal{C}(n))$ at every model size n . We refer to the width of this latency shift as the *efficiency gap*.

3.2. Visualizing Efficiency

The previous section unified the concepts of model efficiency, latency, and computational efficiency. Now we visualize them with the *efficiency gap plot* in Figure 1. We introduce it by way of comparison between two well known convnet models.

EfficientNet [63] set a new state-of-the-art in convnet model efficiency, using fewer operations than existing models while achieving higher accuracy. In practice, however, it ran slower than many older models on GPUs with available inference engine software.

ConvNeXt [46] promised to modernize and simplify convnets; and to provide a new baseline for comparison to vision transformer (ViT) models [15]. ConvNeXt was soon recognized for its speed, and it served as a practical alternative to EfficientNet.

Figure 1.a. shows model efficiency \mathcal{E}_m for both networks, with model size (MACs) on the x-axis and ImageNet classification accuracy (%) on the y-axis. This type of plot is well known from seminal papers addressing the issue of model efficiency, including MobileNet [27], MobileNetV2 [59], and EfficientNet [63]. We observed that EfficientNet has better model efficiency than ConvNeXt because it achieves greater accuracy with fewer operations (MACs).

We added a second x-axis to Figure 1.a. to show ideal latency (milliseconds) and computed it with Equation (1). Ideal latency builds a bridge between model efficiency and actual latency in subsequent plots.

We used peak arithmetic throughput $\mathcal{R}_i = 76.7$ for our NVIDIA Ampere A5000 GPU (GA102 [52]) with base clock frequency 1.17 GHz, which is less than the boost clock frequency of 1.695 GHz. We also set the memory clock to 1.25 GHz, which is less than the peak 2.0 GHz. The clock reductions make the GPU performance stable during benchmarking while keeping the op:byte ratio close to that which would be achieved at full clock speed. We used a batch of 128 images, which is a typical workload for benchmarks on large GPUs.

Recognizing that arithmetic complexity (MACs) is an imperfect predictor of latency, researchers switched to latency as the primary optimization objective [65]. Figure 1.b. plots the accuracy of EfficientNet and ConvNeXt versus their latency measured with

PyTorch Inductor software on the A5000 GPU. ConvNeXt has better actual efficiency than EfficientNet in this experiment because it achieves greater accuracy at lower latency.

The dissonance between model efficiency and latency has vexed deep learning practitioners in recent years. One might be excited by a paper that claims extraordinary model efficiency only to be frustrated by the high latency of the deployed model. Skepticism has grown about the relevance of model efficiency.

Researchers found a reasonable approach: include both model efficiency and latency plots when reporting results [12]. We go a step further by plotting both metrics on the same axes and showing the relationship between them.

Figure 1.c. combines Figures 1.a. and 1.b. by joining the ideal latency axis with the actual latency axis. Both axes have units of milliseconds, so they can simply be merged. The model efficiency and actual efficiency curves appear side-by-side on the same axes. For each model sample, we plot the accuracy on the y-axis and the ideal and actual latencies on the x-axis. A line between the ideal and actual latencies shows the width of the efficiency gap.

Figure 1.d. repeats the same plot using logarithmic scale on the x-axis. We calculated the computational efficiency using Equation (7) for each model sample and labeled the efficiency gaps with the corresponding computational efficiency.

Figure 1.d. shows that large differences between model efficiency and actual latency are caused by low computational efficiency. EfficientNet’s computational efficiency ranges from 5% to 8% in our experiments, and its efficiency gap is much wider than its model efficiency advantage over ConvNeXt. Therefore, computational efficiency can be the dominant factor contributing to latency.

Also of interest is the fact that ConvNeXt’s computational efficiency, at 35% or less, is unimpressive in absolute terms, despite being relatively greater than EfficientNet’s.

These plots help us understand the factors that contribute to the performance difference between EfficientNet and ConvNeXt. They show that poor computational efficiency undermines great model efficiency. They document in precise analytical detail the source of the deep learning practitioner’s frustration with model efficiency.

These plots also suggest that the middle-road on which ConvNeXt travels is sub-optimal, as neither its model efficiency nor its computational efficiency is great. Best performance requires co-optimization of model efficiency and computational efficiency. Is it possible to excel at both? To answer this question, we must first understand computational efficiency.

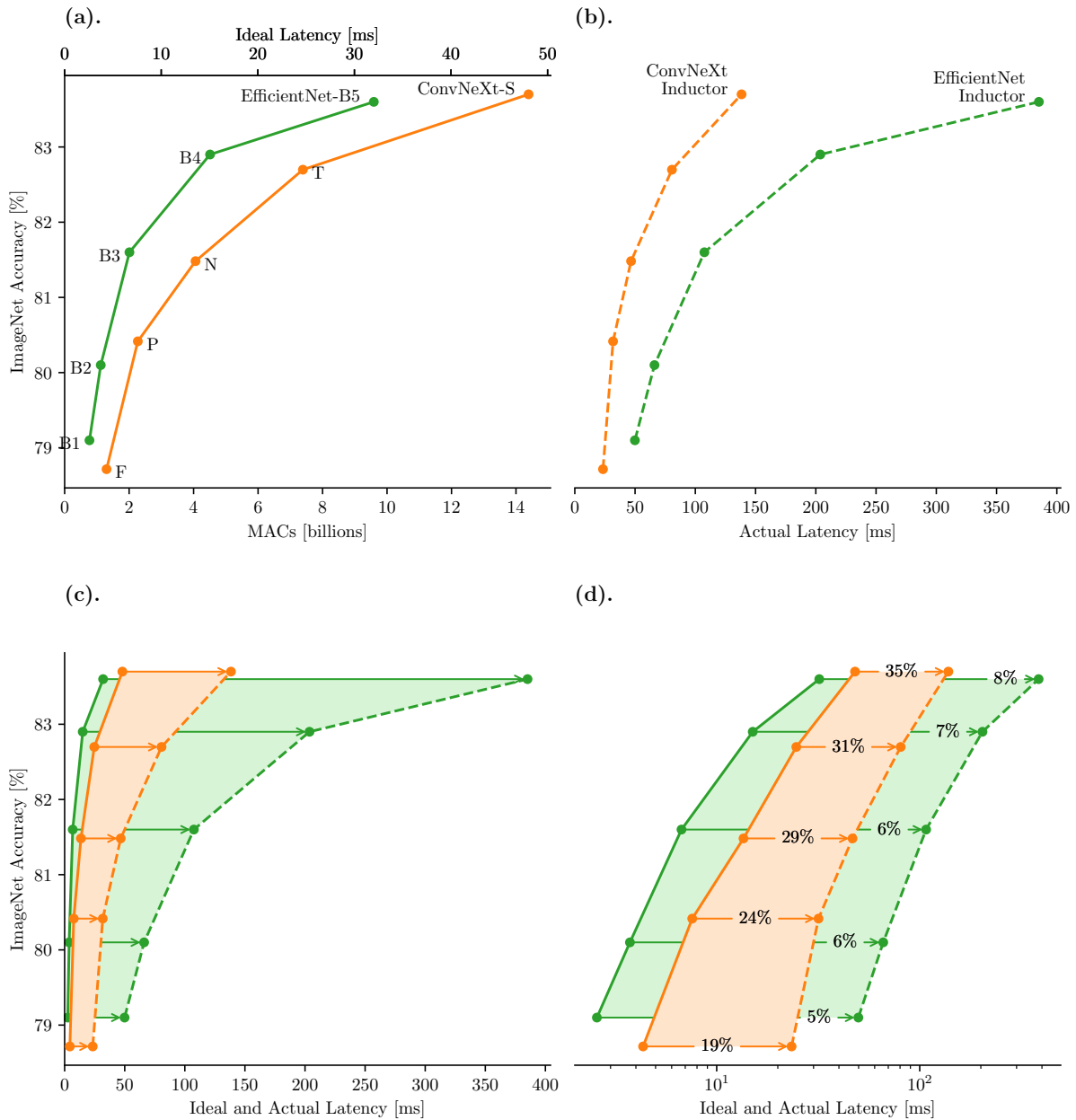


FIGURE 1. Efficiency gap plots illustrate the difference between ideal and actual performance for different models and software. They help us understand the separate contributions of model efficiency and computational efficiency. This figure shows ImageNet-1K classification accuracy and latency for EfficientNet and ConvNeXt using an NVIDIA Ampere A5000 GPU with 76.7 TFLOP/s peak arithmetic throughput running PyTorch Inductor software. Batch size equals 128. **(a).** *Model efficiency* measures accuracy as a function of the number of multiply-accumulate operations (MACs) performed. Dividing MACs by peak arithmetic throughput of the processor yields *ideal latency*, the lowest possible latency for the number of operations. **(b).** *Actual efficiency* measures accuracy versus *actual latency* for a combination of model and software. **(c).** Overlaying model and actual efficiency graphs reveals the *efficiency gap*, the offset between ideal and actual latency. **(d).** Measured with a logarithmic scale on the latency axis, the (negative) width of the efficiency gap equals the logarithm of *computational efficiency*, the ratio between actual and ideal performance. EfficientNet’s poor computational efficiency creates a wide efficiency gap, resulting in longer latency than ConvNeXt, despite superior model efficiency.

4. Waterline: A Simple Performance Model for a Sequence of Parallel Kernels

Williams et al. [72] introduced the *roofline* model to capture the idea that modern multi-processors have an increasingly high ratio of peak arithmetic throughput to DRAM memory bandwidth, and this imbalance presents the first hurdle that a parallel kernel must clear in order to be computationally efficient.

We find that the roofline model explains most of the performance problems with contemporary inference engine software and use it as the foundation for a simple performance model that predicts the efficiency of a sequence of parallel kernels.

We adopt the formulation of the roofline model found in NVIDIA's *GPU Performance Background User's Guide* [49]. *Op:byte* measures the ratio of peak arithmetic throughput to DRAM memory bandwidth for a particular computer. *Operational intensity* measures the ratio of operations performed (OPs) to bytes transferred between DRAM and the processor for a parallel kernel [72]. We count a single multiply-accumulate operation as two OPs [51].

If the operational intensity of a kernel is less than the op:byte ratio of the computer, then the kernel's performance will be limited by the DRAM memory bandwidth. Therefore, the roofline model says that the maximum attainable arithmetic throughput for a parallel kernel is

$$(10) \quad \mathcal{R}_{\max} = \min(\mathcal{R}, \mathcal{B} \frac{n}{b})$$

where \mathcal{R} is the peak arithmetic throughput, \mathcal{B} is the peak DRAM memory bandwidth, n is the number of operations, b is the number of bytes transferred, and $\frac{n}{b}$ is the operational intensity [72].

This formula implies that the minimum attainable latency for a parallel kernel is

$$(11) \quad t_{\min} = \frac{n}{\min(\mathcal{R}, \mathcal{B} \frac{n}{b})}$$

The minimum attainable latency for a sequence of parallel kernels i is

$$(12) \quad T_{\min} = \sum_i t_i = \sum_i \frac{n_i}{\min(\mathcal{R}, \mathcal{B} \frac{n_i}{b_i})}$$

The minimum attainable latency implies the maximum computational efficiency

$$(13) \quad \mathcal{E}_{\max} = \frac{N}{T_{\min} \mathcal{R}}$$

where

$$(14) \quad N = \sum_i n_i$$

is the total number operations across all kernels.

We visualize Equation (12) as a sequence of kernels, side-by-side on a time axis, each of them reaching upwards with height equal to its operational intensity. If a kernel reaches above the processor’s op:byte *waterline*, then it is compute bound, and can attain maximum performance. Otherwise, the “underwater” kernel is memory bound, and its performance is limited by low operational intensity. Figure 3 plots the waterline performance for a number of baseline models.

In Appendix B we derive an extension to Amdah’s Law using waterline analysis.

4.1. Waterline Analysis of Conv2d Layers

Convolutional neural networks are composed of conv2d layers. In this section we examine the function computed by conv2d and analyze its operational intensity.

4.1.1. Conv2d and its Degenerate Cases

The conv2d layer is defined by

$$(15) \quad Y_{nhwk} = \sum_r^R \sum_s^S \sum_c^C A_{krsc} X_{n(h+r)(w+s)c} + b$$

for input tensor $X \in \mathbb{R}^{N \times H \times W \times C}$, weights tensor $A \in \mathbb{R}^{K \times R \times S \times C}$, bias vector $b \in \mathbb{R}^K$, and output tensor $Y \in \mathbb{R}^{N \times H \times W \times K}$; where N is the batch size (i.e., the number of images to be processed in parallel), C is the number of input channels, $H \times W$ is the size of the input and output feature maps, K is the number of output channels, and $R \times S$ is the size of the convolution kernel. Typically, X is padded (implicitly with $\lfloor \frac{R}{2} \rfloor$ and $\lfloor \frac{S}{2} \rfloor$ zeros on the top-bottom and left-right borders, respectively) to support the receptive field of the convolution kernel.

One understands Equation (15) as a convolution nested inside of a matrix multiplication, with matrices $A \in \mathbb{R}^{K \times C}$ and $X \in \mathbb{R}^{C \times N}$, matrix elements $w_{kc} \in \mathbb{R}^{R \times S}$ and $x_{cn} \in \mathbb{R}^{H \times W}$, and element multiplication implemented by 2d convolution [8]. Conversely, it is a matrix multiplication nested inside of a convolution, where the operands are 2d images, the image elements are matrices, and element multiplication is implemented by matrix multiplication [8]. These formulations lend themselves to arithmetic complexity reduction using fast matrix multiplication and fast convolution algorithms [8, 41]. The fast algorithms are most efficient when all the tensor dimensions are large, because the cost of the algorithms' transforms are amortized over the size of the tensor dimensions [8, 41]. Fast algorithms can still be efficient for small tensor dimensions with specialized hardware acceleration, especially if the transforms only use additions and arithmetic shift operations.

Early convnets were composed of stacks of conv2d layers with kernel size equal to 3×3 or larger. Conv2d layers are separated by element-wise nonlinear activation functions (e.g., ReLU [23, 31], SiLU [16, 58]) and pooling layers that downsampled the feature maps to half resolution [42, 31], sometimes merely by subsampling [5, 24]. ResNet34 was the zenith of these early convnets [24]. The ResNet *residual block* is shown in Figure 2(a).

ResNet50 contributed the *bottleneck block* with *point-wise* convolutions; a degenerate case of the conv2d layer with kernel size equal to 1×1 . Setting $R = S = 1$ simplifies Equation (15) to

$$(16) \quad Y_{nhwk} = \sum_c^C A_{kc} X_{nhwc} + b$$

which is just the C-mode (matrix) product (i.e., tensor multiplication [36, p. 460] in the channels dimension) of the weights matrix and input tensor, equivalent to the matrix multiplication

$$(17) \quad Y_{pk} = \sum_c^C A_{kc} X_{pc} + b$$

where dimensions $N \times H \times W$ have been unfolded into a single dimension, P . The bottleneck block is shown in Figure 2(b).

ResNeXt [73] generalized the conv2d operator such that the input and output tensors are divided into groups of channels, and weights connect inputs to outputs in the same

group. This *grouped convolution* can be written as

$$(18) \quad Y_{nhwk} = \sum_r^R \sum_s^S \sum_t^T A_{krst} X_{n(h+r)(w+s)(g(k)T+t)} + b$$

where G is the number of groups, $T = C/G$ is the width of each group, $A \in \mathbb{R}^{K \times R \times S \times T}$ is the weights tensor, and the group index $g(k) = \lfloor \frac{kC}{KT} \rfloor$. Grouped convolutions can be understood as conv2d layers with block-diagonal weights tensors. Equation (15) is a special case of Equation (18) with one group ($G = 1$) and C channels per group ($T = C$). Figure 2(c) shows the ResNeXt block.

Xception [7] and MobileNet [27] used the degenerate case of grouped convolutions where the group width equals a single channel. This *depth-wise convolution* equals

$$(19) \quad Y_{nhwk} = \sum_r^R \sum_s^S A_{krs} X_{n(h+r)(w+s) \lfloor kC/K \rfloor} + b$$

and in the common case where $K = C$,

$$(20) \quad Y_{nhwc} = \sum_r^R \sum_s^S A_{crs} X_{n(h+r)(w+s)c} + b$$

MobileNetV2 [59] used an *inverted residual* block with depth-wise convolution. The MBConv block is pictured in Figure 2(d).

4.1.2. Operational Intensity of Conv2d

The arithmetic complexity of the conv2d layer is

$$(21) \quad n = 2(NHWK)(CRS) + K$$

operations. We can understand this equation as counting CRS multiply-accumulates for every element of the output tensor and K additions for the bias vector.

In the general case of grouped convolution with group-width T , Equation (21) becomes

$$(22) \quad n = 2(NHWK)(TRS) + K$$

operations, or TRS multiply-accumulates per output.

Assuming the conv2d kernel performs only *compulsory loads* [25], we reason that it loads every element of the weights tensor from DRAM exactly once. This assumption is valid for devices with cache that is large enough to hold the weights tensor of a single layer, which is true for the models and devices considered in this paper.

We also assume that every input element is read from DRAM once and every output element is written to DRAM. This assumption is true if the on-chip memory is too small to hold the input and output activation tensors. For now we consider this to be a simplifying assumption, and it will guide us towards novel memory-efficient algorithms in the later sections of the paper.

The input tensor has $NHWC$ elements, the output tensor has $NHWK$ elements, the weights tensor has $KCRS$ elements, and the bias vector has K elements. For grouped convolution, the weights tensor has $KTRS$ elements. Therefore, the general conv2d kernel transfers a total of

$$(23) \quad b = NHWK + NHWC + KTRS + K$$

elements between the processor and DRAM.

We additionally assume that the input tensor is relatively large with $NHW \gg TRS$. We accomplish this in practice by setting $N = 128$ for all subsequent experiments. Other papers that measure vision network latency also used a large batch size [56, 71, 64, 6, ...].

Large batch size is a good fit for the large number of processors found in discrete, desktop GPUs. It is practical for server-side, batched processing of images, but not for real-time vision systems. Again, this choice is a simplifying assumption that we will revisit.

Thus the operational intensity of conv2d with float16 arithmetic and two bytes per element equals

$$(24) \quad \begin{aligned} \frac{n}{b} &= \frac{(NHWK)(TRS) + K/2}{NHWK + NHWC + KTRS + K} \\ &\approx \frac{TRS}{1 + \frac{C}{K} + \frac{TRS}{NHW}} \\ &\approx \frac{TRS}{1 + \frac{C}{K}} \quad \text{if } NHW \gg TRS \end{aligned}$$

where we assumed that the number of input and output elements per channel, NHW , is much greater than the number of operations per output, TRS . This also implies that

the activation tensors dominate the DRAM transfers.

Each of the degenerate cases of the conv2d layer reduces the number of operations and the size of the weights tensor without changing the size of the input and output tensors. Reduced arithmetic complexity causes the operational intensity to decrease relative to the full conv2d layer. Figure 2 shows the evolution of convnet blocks and the operational intensity of their conv2d layers.

According to Equation (24), the full conv2d layer with $T = C$ has operational intensity

$$(25) \quad \frac{n}{b} \approx \frac{CRS}{1 + \frac{C}{K}}$$

while point-wise convolution has $R = S = 1$ and $T = C$, yielding

$$(26) \quad \frac{n}{b} \approx \frac{C}{1 + \frac{C}{K}}$$

and depth-wise convolution has $T = 1$, giving

$$(27) \quad \frac{n}{b} \approx \frac{RS}{1 + \frac{C}{K}}$$

Thus full conv2d has approximately RS times the operational intensity of point-wise convolution and C times the operational intensity of depth-wise convolution. Also, it is worth noting that the operational intensity of grouped and depth-wise convolution is approximately independent of the number of channels, C .

As mentioned, we assume that NHW is large in subsequent analyses, which we accomplish by setting the batch size $N = 128$. In real-time systems that require small batch size, possibly $N = 1$, the convnet model is typically used as a backbone for an object detection or semantic segmentation network that usually requires high resolution images for acceptable accuracy. Still, an input image as small as $512_H \times 512_W$ will only produce a $16_H \times 16_W$ activation tensor in the last stage of a typical convnet backbone. So it is worth examining the possibility NHW is small.

If NHW is approximately equal to TRS , then both terms contribute to the operational intensity in Equation (24). Conceptually, the data movement incurred by the weights and input and output activations are all significant. In the extreme, when $T = C$ and $NHW \ll CRS$, then Equation (24) yields

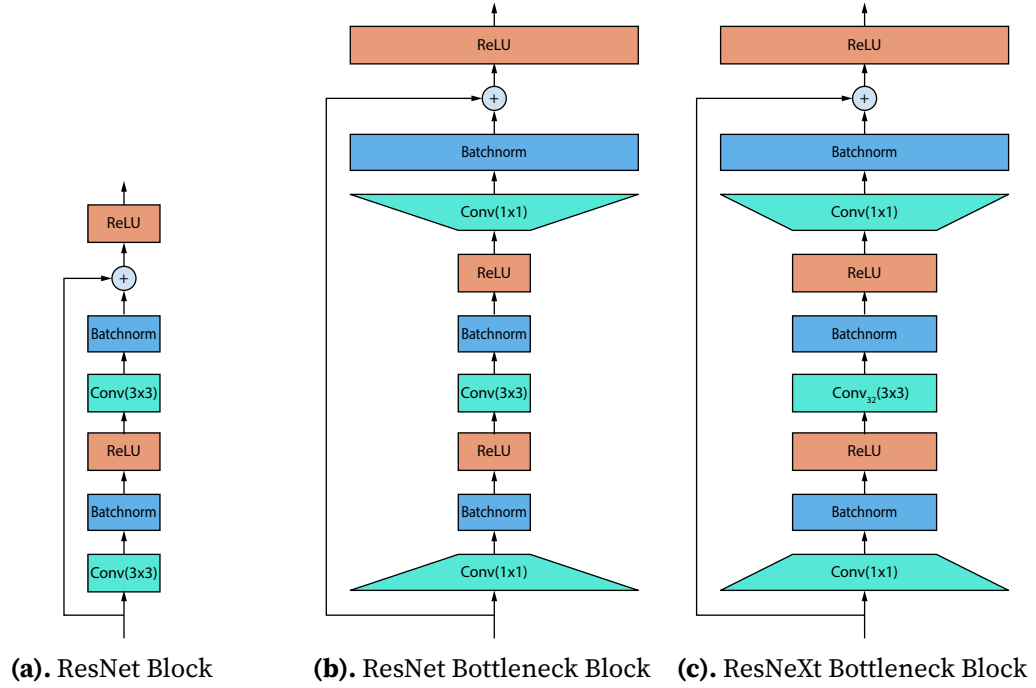
$$(28) \quad \frac{n}{b} \approx NHW$$

Typically this case would apply when $NHW \ll C$. We can understand this equation as saying that the cost of loading the weights tensor is amortized over the pixels in the activation tensor, if that number is small relative to the width of the network. Real-time systems that require a small batch size in order to minimize latency might benefit from increasing input image resolution $H \times W$. They could also use smaller width (C) to maintain the total number of operations.

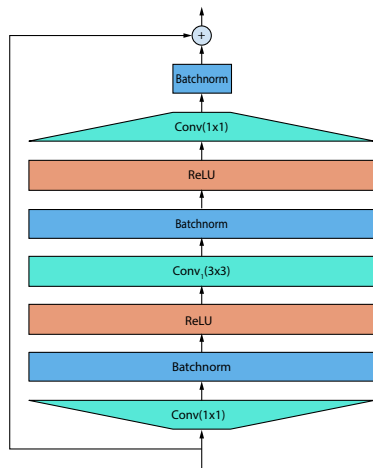
4.1.3. Degenerate Conv2d and the op:byte Waterline

Figure 2(e) plots the operational intensity of different types conv2d layers versus the number of input channels, C . For reference, it also shows the op:byte ratio of our baseline processor, the NVIDIA A5000 GPU. We see that the full conv2d layer with $R = S = 3$ has relatively large operational intensity even for a small number of channels. Point-wise convolution with bottleneck expansion ratio equal to four ($\frac{K}{C} = 4$) is “underwater” until the number of channels reaches a relatively large number. Grouped convolution with $T = 32$, as used by ResNeXT101_32x4d, has a flat operational intensity that is underwater. Depth-wise convolution with $R = S = 3$ has operational intensity close to zero.

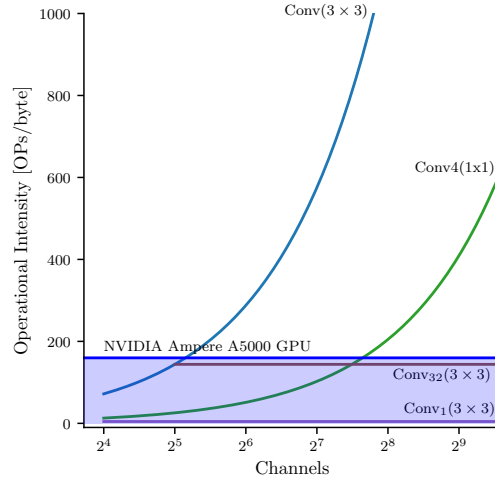
Because on-chip SRAM has greater bandwidth than off-chip DRAM, hardware designers can improve the computational efficiency of memory-bound kernels by increasing the SRAM size until all the activations fit on-chip. However, SRAM size contributes to the die size which determines cost. A kernel that uses a larger workspace requires a greater die size to achieve the same arithmetic throughput. It achieves its performance at a greater cost than a kernel that uses memory efficiently.



(a). ResNet Block (b). ResNet Bottleneck Block (c). ResNeXt Bottleneck Block



(d). MBConv Inverted Bottleneck



(e). Conv2d Operational Intensity vs. Channels

FIGURE 2. Evolution of convnet blocks and convolutional layers. (a). ResNet34 used *residual blocks* with conv2d layers: Conv(3 × 3). **(b).** ResNet50 added *bottleneck blocks* with an expansion ratio equal to four using *point-wise* convolutions: Conv₄(1 × 1). **(c).** ResNeXT101_32x4d used grouped-convolutions with group-width equal to 32: Conv₃₂(3 × 3). **(d).** MobileNetV2 used *inverted residual blocks* with *depth-wise* convolutions: Conv₁(3 × 3). **(e).** Operational intensity of convnet layers as a function of the number of channels. The Conv(3 × 3) layers used by early convnets had large operational intensity. Point-wise, grouped, and depth-wise convolutions progressively decreased the operational intensity of conv2d layers.

4.2. Waterline Analysis of Convnet Models

In this section we use Equation (12) to investigate the minimum attainable latency of different convnet models.

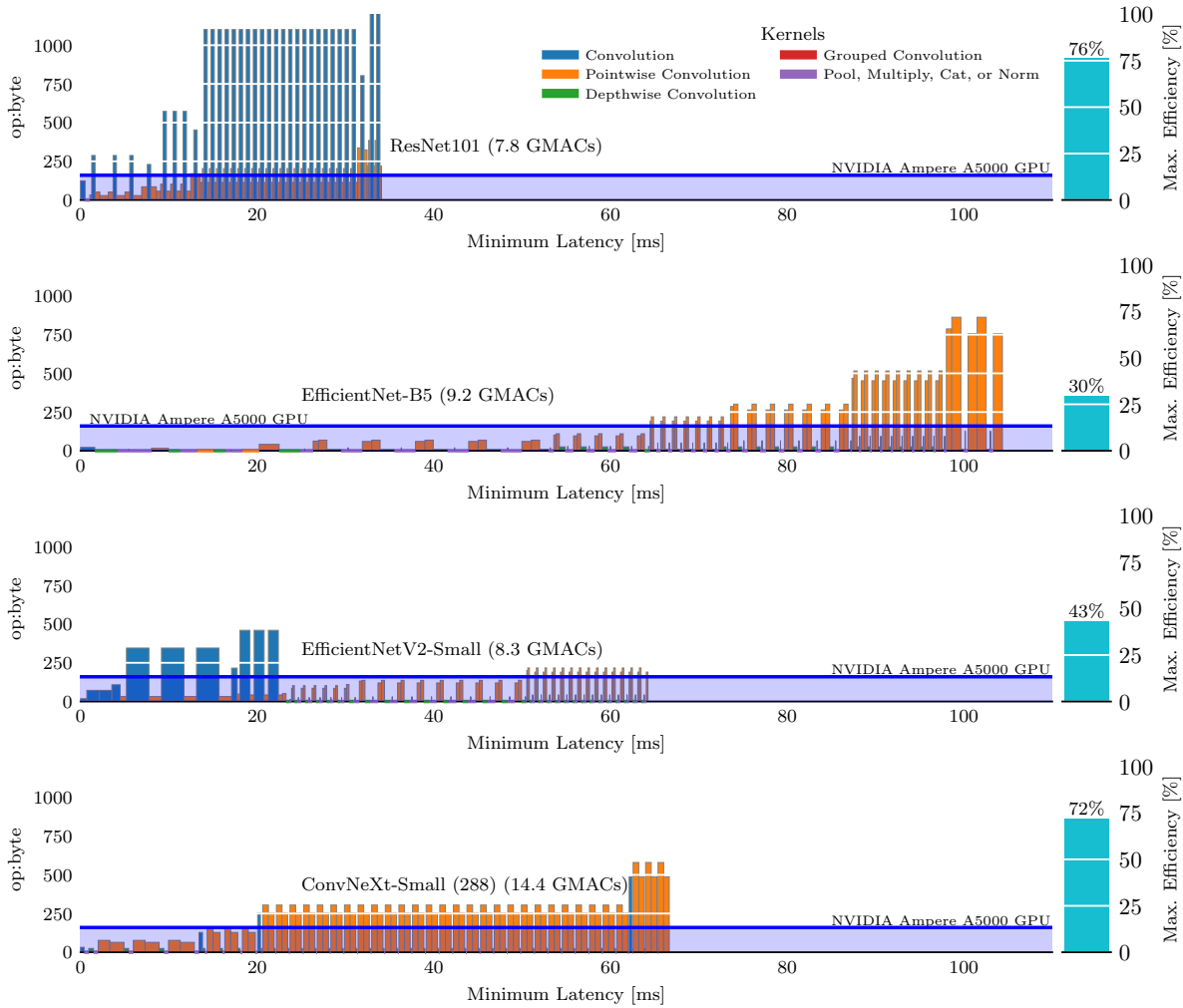


FIGURE 3. Waterline analysis of baseline models. These plots compare the operational intensity of individual layers with the op:byte waterline of the NVIDIA Ampere A5000 GPU. Single-layer kernels are often memory bound because their low operational intensity is “underwater.” Memory bound kernels have higher attainable latency and lesser attainable computational efficiency (max efficiency). Again, we used float16 arithmetic and batch size equal to 128.

Figure 3 shows the minimum attainable latency and the corresponding maximum computational efficiency for baseline convnet models. We plot the operational intensity of each kernel on the y-axis and the corresponding minimum attainable latency on the x-axis. Kernels that rise above the processor’s op:byte *waterline* are compute bound,

others are memory bound. We also compute the maximum computational efficiency for each network (with Equation (13)) and show it next to the waterline plot.

We assume layer-by-layer execution of the network, while allowing for trivial operator fusions that combine convolution, bias, residual shortcut addition, and activation functions in a single kernel. These are the simple kernel fusions implemented in PyTorch Inductor and other available inference engines.

Figure 3 predicts relatively high maximum efficiency for ResNet101 and ConvNeXt-Small, which agrees with the popular sentiment that those models are computationally efficient in deep learning frameworks.

ResNet101 has many conv2d layers with large operational intensity. It also has many point-wise convolution layers that vary from low operational intensity in the early stages of the network to moderate operational intensity in the late stages where the number of channels is greater.

ConvNeXt-Small has many point-wise convolution layers with large operational intensity due to the fact they use a large number of channels. It also has depth-wise convolution layers with extremely low operational intensity, but these transfer relatively little data, because they are placed at the block’s bottleneck where the activations tensor has fewer channels.

EfficientNet-B5 has relatively low maximum attainable efficiency because of the small number of channels in the early stages of the network. Also, it has depth-wise convolution layers with low operational intensity, and these layers operate on the hidden-layer tensors in the bottleneck blocks where the number of channels is greatest.

These results suggest that narrow (small number of channels per layer) models are computationally inefficient. This observation agrees with the work of Dollar et al. [14] who saw that computational efficiency decreases as the number of network activations increases. They reasoned that models should have more channels and fewer layers to increase the ratio of activations to operations. We understand this as a simple strategy to increase the operational intensity of point-wise convolutions.

But this creates a dilemma, because the narrower and deeper models like EfficientNet have greater model efficiency. Ideally one could improve computational efficiency without sacrificing model efficiency.

4.3. Mediant Operational Intensity

Several papers applied the roofline performance model directly to an entire neural network [43, 33, 32, ...]. These papers computed the operational intensity of a network

simply by dividing the total operations by the total bytes transferred to and from DRAM,

$$(29) \quad \text{mediant operational intensity} = \frac{\sum_i n_i}{\sum_i b_i}$$

for layers i , with n_i operations and b_i bytes transferred per layer. Mathematicians recognize Equation (29) as the *mediant* of the fractions $\frac{n_i}{b_i}$. The term originates from the inequality $\frac{a}{b} < \frac{a+c}{b+d} < \frac{c}{d}$ [22, 18].

If we were to interpret Equation (29) as the operational intensity of a set of kernels, then we would infer that the kernels run concurrently. The roofline model requires this assumption, because the latency of computation cannot hide the latency of data movement unless both run concurrently.

Otherwise, if the kernels run sequentially, then Equation (29) only approximates the waterline performance model presented earlier. It is correct when the kernels are all memory-bound or all compute-bound. But it overestimates the attainable performance of a sequence that has both memory-bound and compute-bound kernels. Because Equation (29) adds the excess operations of the compute-bound kernels to the operations of the memory-bound kernels, the sequence appears to be less memory-bound than it truly is.

How accurate is Equation (29) when applied to a convnet? Figure 4 plots the maximum attainable efficiency of different convnets versus the processor op:byte ratio. It shows both the roofline and waterline performance models. Again, we use batch size equal to 128 and 2 bytes per tensor element. For processors with very high op:byte ratios, all layers of the convnets are memory bound, and the roofline model (using the mediant operational intensity) agrees with the waterline model. For low to moderate op:byte ratios, the roofline model evaluates the convnets as compute bound, while the waterline model recognizes that some of the layers are memory bound. This discrepancy causes the roofline model to overestimate the attainable efficiency.

For models like ResNet101 and ConvNeXt-Small, which have some layers with relatively high operational intensity, roofline drastically overestimates the attainable efficiency, unless the processor has a very large op:byte ratio. For models like EfficientNet-B5, which have fewer layers with large operational intensity, roofline is closer to the waterline model.

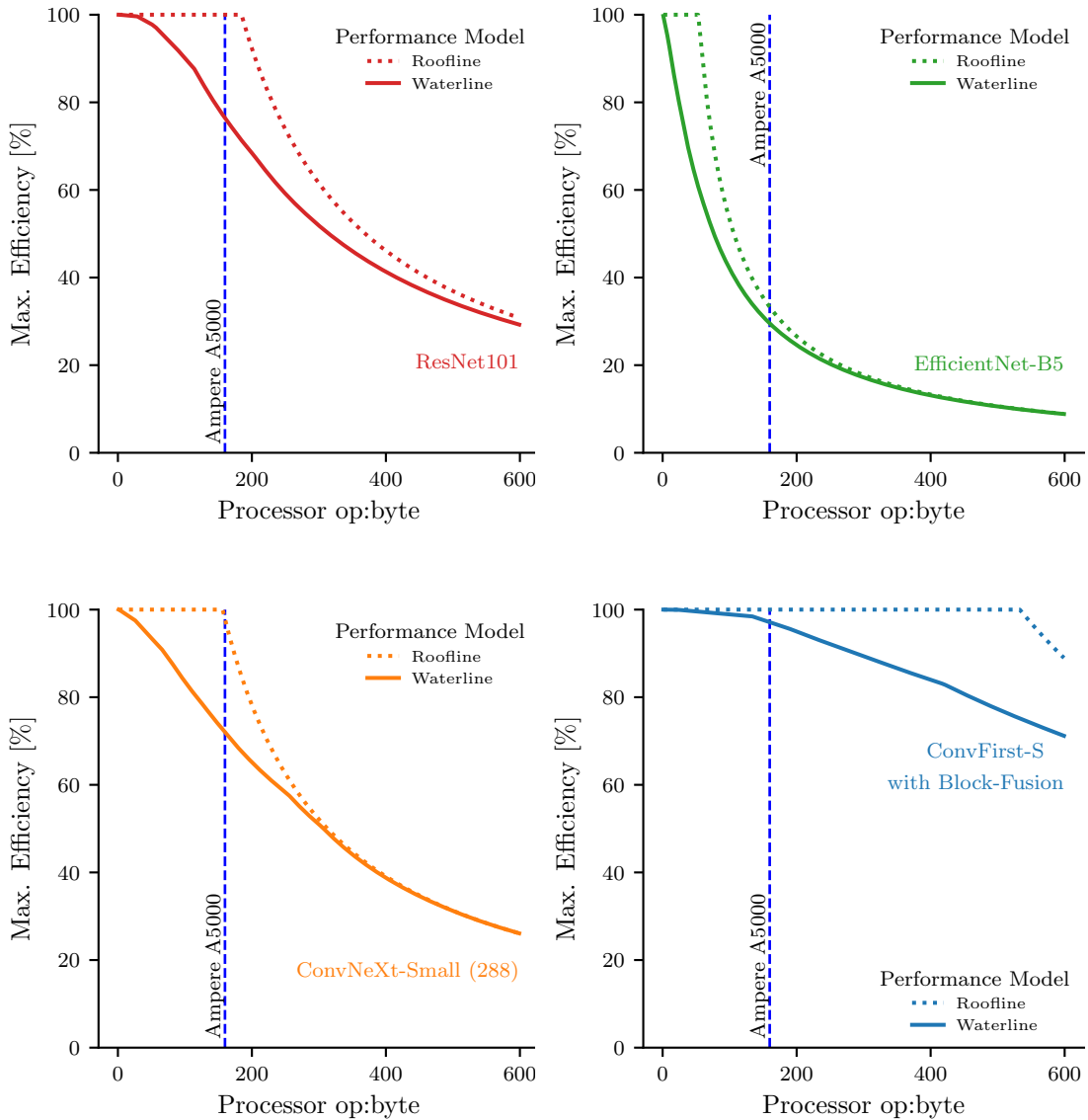


FIGURE 4. Comparison of the attainable computational efficiency calculated by the waterline and roofline performance models. Roofline was originally intended as a performance model for a single parallel kernel [72]. Hence roofline overestimates the attainable efficiency for a sequence of kernels, if some of the kernels are compute bound and others are memory bound. Waterline is accurate regardless, because it measures how each kernel contributes to the minimum latency of the sequence. ConvFirst is our new model. See Section 6 for details.

5. Block Fusion: An Optimization for Degenerate Conv2d Layers

In this section, we improve the operational intensity of inverted residual blocks by fusing their layers into a single kernel. We find a path through each block’s computational graph that creates temporal locality and avoids DRAM memory transfers. The inverted residual block becomes a module with low-bandwidth interface and computationally dense implementation. We call this technique *block fusion*.

Block fusion is faster than layer-by-layer execution, because the degenerate conv2d layers used in modern convnets have low operational intensity when computed separately.

To navigate the complex space of kernel designs, we introduce a simple computational model called the “tensor machine.”

5.1. Tensor Machines

We believe that the complexity of low-level source code obscures the high-level algorithmic ideas that are essential for efficient kernels. We devised the tensor machine as a picture language for drawing simple kernel diagrams that capture the essence of our efficient algorithms.

The *tensor machine* is a simple abstract computer that helps us visualize kernels and analyze their theoretical efficiency. It uses simple high-level operations that act on tensors and places each tensor in DRAM, global memory, or local memory. Tensor machines define a kernel by showing its operations and data movement using the symbols in Figure 5.

Tensor machine operations include matrix multiplication (or channels-mode product of an activation tensor and a weights matrix [36, p. 460]), grouped conv2d, element-wise multiplication, activation functions, and global average pooling.

The tensor machine’s three memory regions are DRAM, global memory, and local memory. DRAM is slow, off-chip memory with large capacity. Global memory is on-chip memory that is accessible by all processors. Local memory is fast on-chip memory internal to each processor.

Global memory functions as a cache for weights and overlapping inputs and as a shared memory for inter-processor communication.

Global and local memory have limited capacity. In this paper we merely assume that global memory is sufficiently large to hold the weights of a single residual block and a small number of activations. This assumption is reasonable for all the models in

this paper.

Local memory is only large enough to store small tiles of activations and weights tensors. High-resolution tiles reduce the global memory bandwidth requirement, because more computation is performed for each weight value that is transferred from the global memory cache. In this paper, we defer analysis of the exact local memory capacity and tile sizes to the platform-specific kernel development stage.

We use waterline analysis to compute the minimum attainable latency for a kernel and its tensor machine with a given op:byte ratio. We only count the multiply-accumulate operations of tensor-matrix multiplication and conv2d operators, all other operators do not contribute to the operational intensity. This approximation is useful for neural networks because tensor-matrix multiplications and conv2d operations dominate their arithmetic complexity.

This simple machine facilitates the high-level choices that dominate performance and avoids the low-level details that create complexity.

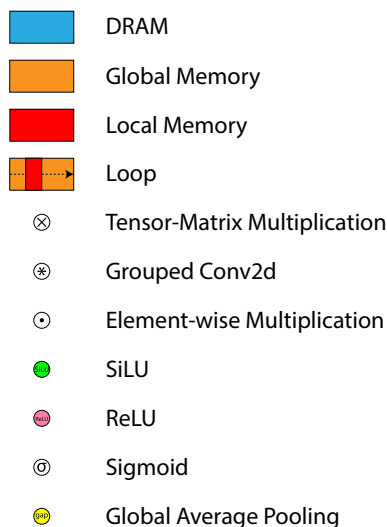


FIGURE 5. The tensor machine is a simple abstract computer for designing convnet kernels. It has three memory spaces: DRAM (slow, off-chip memory), global memory (on-chip memory shared by all processors), and local memory (fast memory internal to each processor). It uses basic high-level operations, including matrix multiplication (or channels-mode matrix product), grouped conv2d, element-wise multiplication, global average pooling, and activation functions. The *loop* symbol indicates a for-loop that iterates over memory tiles, loading one tile at a time into a local memory buffer.

5.2. Feed-Forward Network

Position-wise Feed-Forward Network (FFN) is a block used prominently by Transformers [69] and ConvNeXt [46]. It is also called Multi-Layer Perceptron (MLP) [66]. FFN performs two consecutive linear transformations with an element-wise activation function after the first:

$$(30) \quad \text{FFN}(X) = \phi(XU + a)V + b$$

where $X \in \mathbb{R}^{P \times C}$ is the input, $U \in \mathbb{R}^{C \times \alpha C}$ and $V \in \mathbb{R}^{\alpha C \times C}$ are the weights, $a \in \mathbb{R}^{\alpha C}$ and $b \in \mathbb{R}^C$ are the bias, and ϕ is an activation function, with P as the number of samples, C as the number of channels, and α as the expansion factor.

The most direct algorithm to compute FFN operates layer-by-layer, first computing hidden layer $Y \in \mathbb{R}^{P \times \alpha C}$ as

$$Y = \phi(XU + a)$$

then computing output $Z \in \mathbb{R}^{P \times C}$ as

$$Z = YV + b$$

The layer-by-layer algorithm creates a large hidden layer Y with α times as many channels as the input and output layers X and Z . In a stack of FFN blocks, reading and writing Y dominates the memory cost of the layer-by-layer algorithm, accounting for $\frac{\alpha}{\alpha+1}$ of all activation memory.

We will derive a memory-efficient algorithm that practically eliminates the hidden layer activations. This algorithm is a special case of the one that was proposed by Sandler et al. for the MBConv block [59].

First, compute a single channel Y^r of the hidden layer by multiplying the input by column U^r of weights

$$(31) \quad Y^r = \phi(XU^r + a_r)$$

and exploiting the fact that ϕ is an element-wise function.¹

Second, multiply channel Y^r by row V_r to form an outer product, and the sum of the products over r equals output matrix Z :

¹For matrix A , we write A_i for row i and A^j for column j [4, p.54].

$$Z = \sum_{r=1}^{\alpha C} Y^r V_r + b$$

Substituting Equation (31) for Y^r yields the complete formula:

$$(32) \quad \text{FFN}(X) = \sum_{r=1}^{\alpha C} \phi(XU^r + a_r)V_r + b$$

Equation (32) defines a memory-efficient algorithm that computes a single channel of the hidden layer, immediately uses it to update the output layer, and then discards it. The algorithm iterates over all hidden channels and reuses the same small workspace to store each of them. Therefore, only a small fraction of the hidden layer exists in memory at any given time.

From an algorithmic standpoint, Equation (32) implements a *loop fusion* optimization [35, p. 254]. In the layer-by-layer algorithm, the first linear transformation loops over $r \in [1 \dots \alpha C]$, producing hidden channels Y^r . The second linear transformation also loops over r , consuming Y^r . The large number of hidden channels αC causes the time elapsed between the production and consumption of Y^r to be large. Therefore, a large workspace is needed to store the full tensor Y . Loop fusion increases temporal locality by producing and consuming each Y^r in the same loop iteration. Both the size of the workspace and the communication cost of the algorithm are reduced.

From a model architecture standpoint, Equation (32) virtually eliminates hidden layer $Y \in \mathbb{R}^{P \times \alpha C}$. The FFN block becomes a single layer with weights $U \in \mathbb{R}^{C \times \alpha C}$ and $V \in \mathbb{R}^{\alpha C \times C}$, input $X \in \mathbb{R}^{P \times C}$, output $Z \in \mathbb{R}^{P \times C}$, no hidden layer, and large operational intensity.

5.3. ConvFirst Block

We designed a convnet block with the goal of exploiting the FFN algorithm from Equation (32). The first layer of the block is a grouped convolution. We chose group width equal to 8 channels because it matches the size of the matrix multiply implemented by the NVIDIA tensor core instruction `mma.m16n8k8.f16` [54]. An FFN layer follows the grouped convolution. A residual shortcut connects the block input to the output, and a batchnorm layer [30] follows each linear layer. The downsampling variant of ConvFirst used BlurPool [76]. Figure 6 shows the block diagrams.

We call the block *ConvFirst* because it puts the convolutional layer before the FFN layers. ConvFirst differs from ResNet and MBConv, which place the convolution in the middle of the block.

Putting the convolution first means that there is no overlap in the receptive fields of the rest of the block’s layers. FFN layers have a one-to-one dependency between input and output pixels. Therefore, we can divide the output tensor into many tiles and compute each of them in parallel without any inter-tile communication or over-compute. Only the input tiles overlap, and the overlap is handled gracefully by the memory cache, so each input value is loaded from DRAM at most once.

ConvFirst uses the ReLU [23, 31] activation function because it can be computed efficiently. The cost of the computation is amortized over the block’s input channels, so an advanced function like SiLU [16, 58] would be relatively expensive if the number of channels were small. ReLU does cause a slight accuracy drop relative to SiLU in our model experiments, and SiLU computation is reasonably efficient on processors that accelerate the tanh special function. Therefore, SiLU might be preferable in larger models.

ConvFirst is very similar to ConvNeXt, which was discovered independently [46]. ConvFirst and ConvNeXt are basically the same block with different normalization, group-width, and kernel-size.

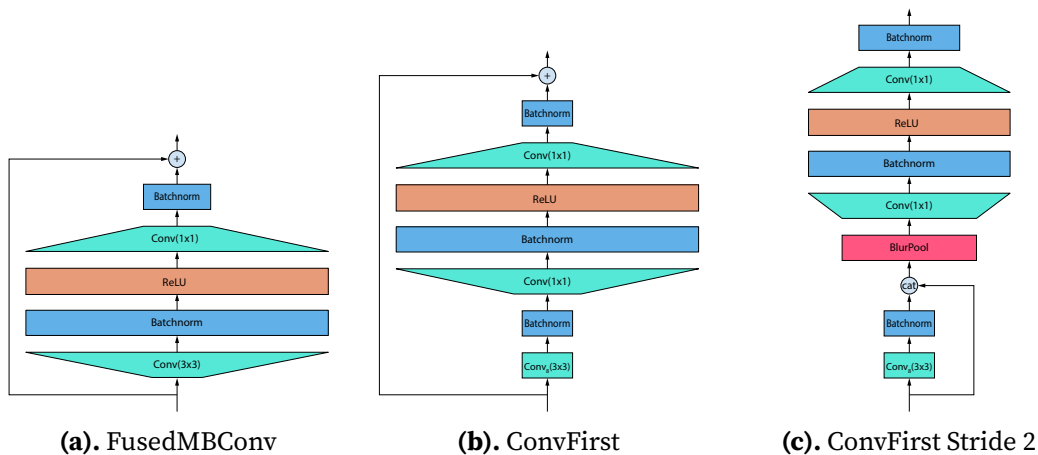


FIGURE 6. (a). The FusedMBConv block, as used in EfficientNet-EdgeTPU [21] and EfficientNetV2 [64], has a conv2d(3×3) layer that uses a large number of arithmetic operations. The block also affords a memory-efficient block-fusion implementation [40]. **(b).** We created the ConvFirst block to be a light-weight mimic of FusedMBConv. ConvFirst also affords block fusion but uses far fewer operations. ConvFirst is very similar to ConvNeXt [46]. **(c).** ConvFirst uses BlurPool [76] for downsampling to improve shift invariance of downstream tasks.

5.3.1. Block-Fusion Kernel for ConvFirst

We designed a tensor machine kernel that implements the ConvFirst block. The *block-fusion* strategy casts the entire block as a single computation with three weights tensors and no hidden activations. Actually each hidden activation exists for a moment in local memory, but it is invisible to the global memory system. Therefore, ConvFirst blocks have low communication cost and large operational intensity, even when the number of channels is small.

Figure 7(a) shows the tensor machine that executes ConvFirst layer-by-layer. This execution plan produces a large DRAM tensor for the hidden-layer activations.

Figure 7(b) shows our block-fusion kernel. It loads an input tile from DRAM into local memory. It computes the grouped-convolution of the input tile and retains the result in local memory. It also initializes the output accumulators with the input-tile values, thereby implementing the residual shortcut connection.

Next it computes the FFN layers using the loop fusion algorithm defined in Equation (32). A single loop over hidden-layer channels produces activations with the first linear transform and projects them onto the output tile with the second. After the last loop iteration, the ConvFirst block is complete and the output tile is stored to DRAM.

Each loop iteration processes a small number of hidden-layer channels, and a small buffer holds the working set in local memory. Gone is the large DRAM buffer that layer-by-layer execution uses.

The block-fusion kernel requires that the number of channels is small enough that the input and output tiles fit in local memory. This requirement is satisfied for the small vision models we create in the later part of this paper and the NVIDIA GPU on which we implement the kernel. It would not be true for large models.

The kernel variant shown in Figure 7(c) scales the block-fusion kernel for a large number of channels. It partitions the input and output tiles channel-wise across two processors. Each processor loads half the input channels and produces half the output channels. A small tensor in global memory accumulates the partial sums produced by each processor to form the hidden-layer channels.

The cost of the add operation in global memory is amortized over the channels of the input and output tensors, so we expect it to be insignificant when the number of channels is large. For a very large number of channels, we would partition them across four or more processors.

Batchnorm layers are constant affine transforms during inference, so we fold them into the weights and bias of the preceding conv2d layer.

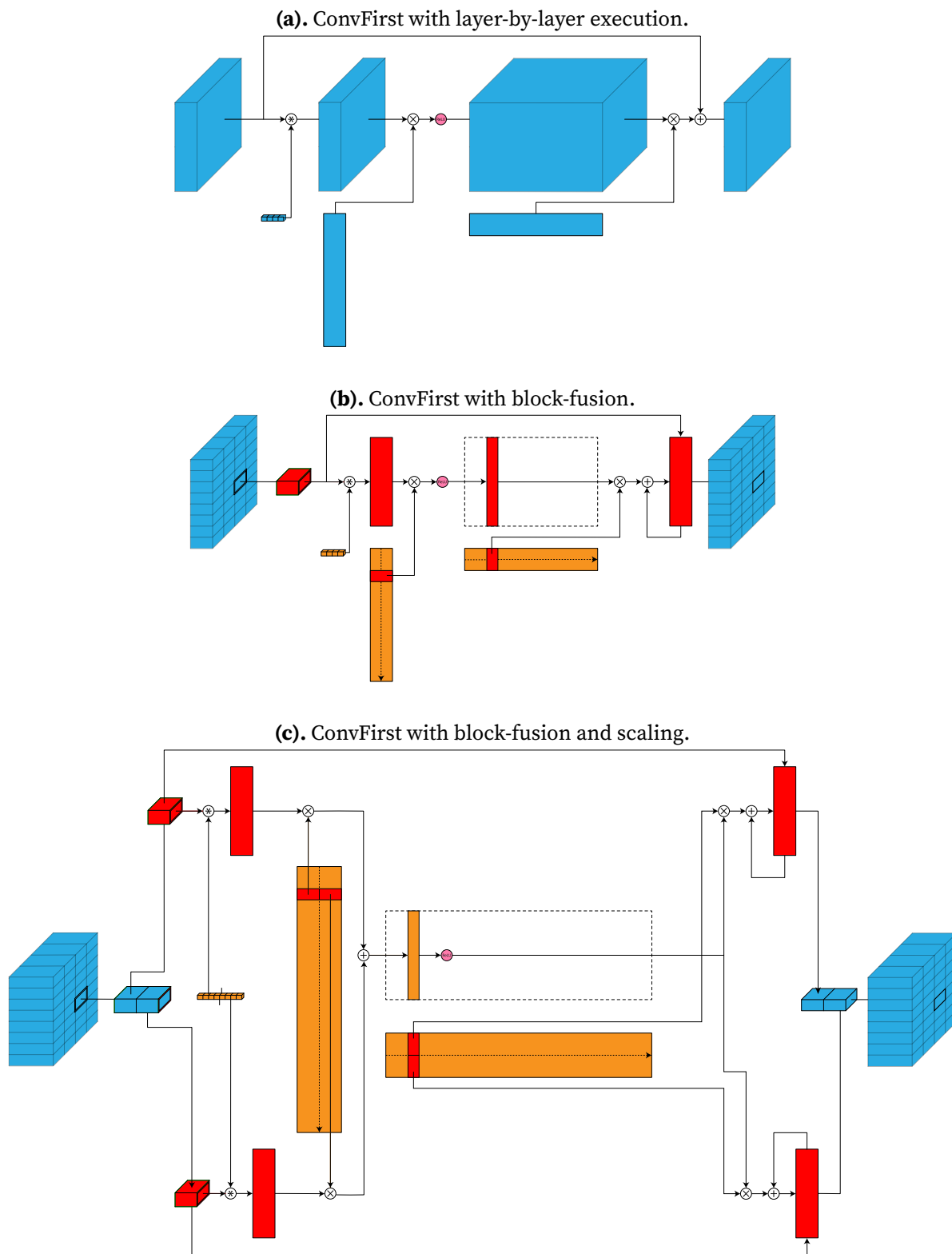


FIGURE 7. Tensor machine for ConvFirst kernels. **(a).** Layer-by-layer execution creates a large tensor in DRAM for the hidden-layer activations. **(b).** Block-fusion computes all layers simultaneously using small tiles in local memory (red). **(c).** Block-fusion scales to support a large number of channels by partitioning the input and output tiles channel-wise across multiple processors. For large NHW , the weights matrices are almost always in global memory (orange) cache.

5.3.2. Waterline Analysis of ConvFirst

Figure 8 shows the waterline analysis of the ConvFirst kernels for a range of block parameters with the op:byte ratio of the A5000 GPU as the waterline. The plot compares the operational intensity and minimum attainable latency for the single-layer kernels and the block-fusion kernel. Each “well” shows the results for a different choice of block parameters.

Single-layer kernels are memory bound for all blocks, while the block-fusion kernels are only memory bound when the expansion ratio (α) is small. When the expansion ratio equals 6, the block-fusion kernels are compute bound for as few as 32 channels. The minimum attainable latency of the block-fusion kernels is significantly lower for all blocks. The speedup is greatest when the number of channels and expansion ratio is smallest, where the point-wise convolutions are severely memory bound.

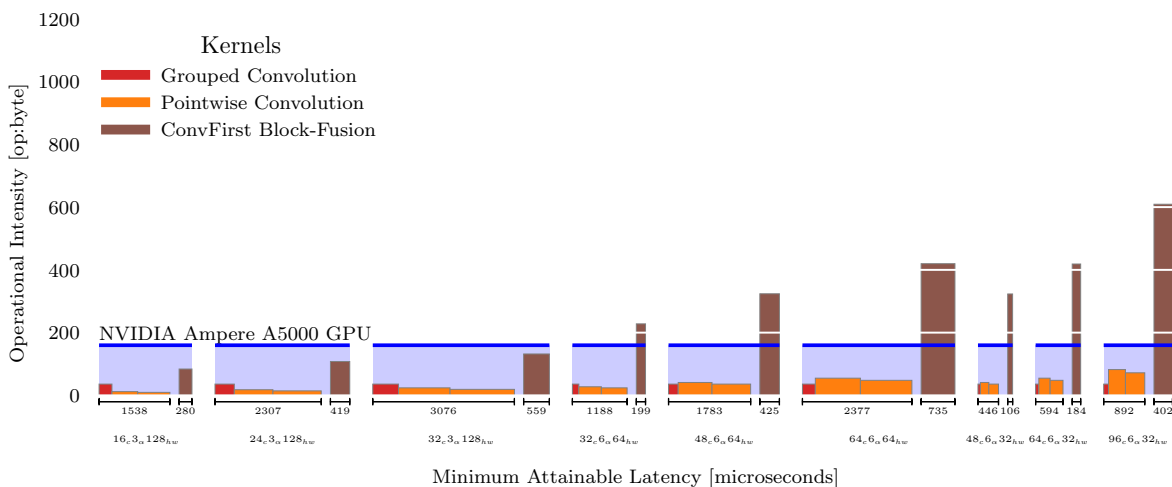


FIGURE 8. Waterline plot for the ConvFirst block with single-layer and block-fusion kernels. The vertical axis shows the operational intensity of the kernels, and the horizontal axis shows the minimum latencies derived from roofline analysis. A horizontal blue line indicates the op:byte ratio (i.e., the *waterline*) of the A5000 GPU. “Underwater” kernels are memory bound. The block-fusion kernels avoid writing the activations of the hidden layer to DRAM. Therefore, they have significantly greater operational intensity and can attain lower latency.

5.4. MBConv Block

The MBConv block was originally developed for MobileNetV2 as a memory-efficient block suitable for convnets that run on small mobile devices [59]. EfficientNet added Squeeze & Excitation layers to the MBConv block and scaled the model to very large

size and accuracy while achieving state-of-the-art model and parameter efficiency [63].

Figure 9 shows our variant of MBConv. We substituted grouped convolution for the traditional depth-wise convolution, to achieve better utilization on matrix multiply accelerators. On NVIDIA GPUs with float16 tensor core arithmetic, we used group-width equal to eight channels.

Our MBConv variant uses BlurPool for downsampling [76]. The purpose of BlurPool is to improve shift invariance in downstream tasks, like object detection and semantic segmentation. In our model experiments, we used BlurPool with the Triangle-3 filter.

The waterline analysis of EfficientNet in Section 4.2 showed that all layers of the MBConv block are memory bound in the early stages of the network, where the number of channels is small. Therefore, we are interested in MBConv for the late stages of the network, where the number of channels is large and the resolution (height and width) of the activation tensor is small. We designed an MBConv block-fusion kernel that targets this hyperparameter domain.

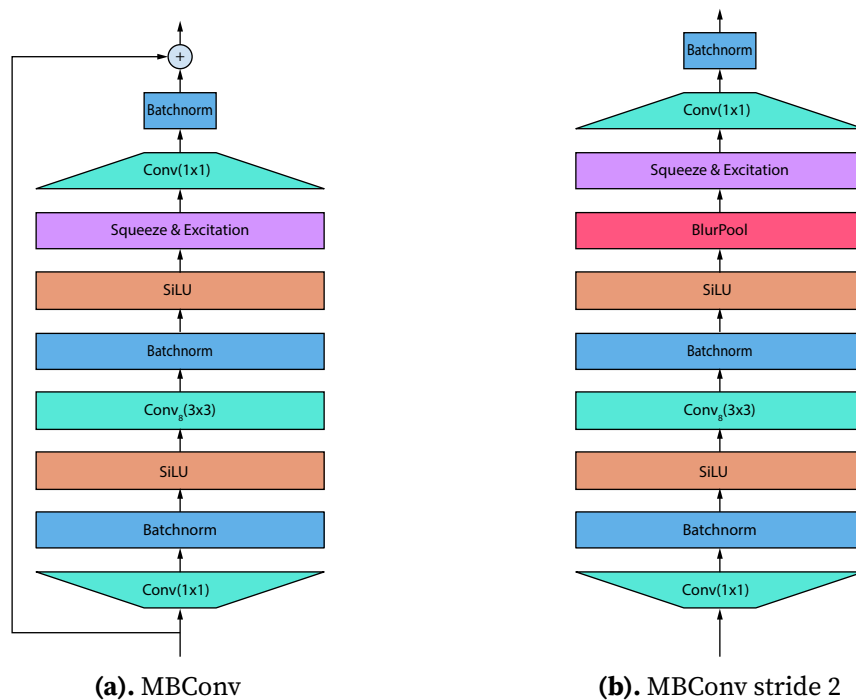


FIGURE 9. MBConv block with Squeeze & Excitation. We modified the traditional MBConv block to use group-width 8 convolution because that operation maps perfectly to NVIDIA tensor cores. We added a BlurPool [76] layer after the grouped convolution layer to implement downsampling.

5.4.1. Block-Fusion Kernel for MBConv

Figure 10 shows the tensor machine for layer-by-layer execution for the MBConv block with Squeeze & Excitation. The tensor shapes are representative of those found in the later stages of a convnet, where the resolution of the activation tensor is low and the number of channels is large. These hyperparameters produce small activation tensors and relatively large weights matrices. For the model sizes considered in this paper, the weights tensors fit in global memory of a contemporary GPU.

We show the weights matrices and activation tensors partitioned into eight blocks each, which correspond with the blocks used by each processor in the block-fusion algorithm, described below.

Figure 11 shows the tensor machine for a block-fusion kernel. We documented this same kernel in a previous article [38].

The block-fusion kernel uses multiple processors, assigning a group of hidden-layer channels to each. Each processor computes its own group of hidden-layer channels using the corresponding block of weights from the first point-wise convolution and storing the activations in local memory. Then it applies the SiLU activation function.

Then each processor computes the grouped convolution on its channels, again applying the SiLU activation function, producing the convolution layer output, which is also stored in local memory. If the width of the grouped convolution evenly divides the number of channels assigned to each processor, then the grouped convolution can be computed in parallel without any inter-processor communication.

Then each processor computes the global average pool of that result, yielding a vector with one value for each channel. That vector multiplies the corresponding block of the squeeze-matrix, producing a partial sum of the squeeze-vector. The vectors produced by all the thread-blocks are added in a buffer in global memory to produce the squeeze-vector. This addition in global memory is a synchronization point for all the thread-blocks.

Then each processor loads the squeeze-vector from the global memory buffer, applies the ReLU activation function, and multiplies it by the block of the excitement matrix corresponding to its channels. A sigmoid activation is applied to the result of that transformation, producing gating values between 0 and 1. These gating values multiply the corresponding channels of the convolution layer output, producing the output of the Squeeze & Excitation layer (SE).

The SE output multiplies the corresponding block of weights from the second point-wise convolution. The result is added on to the MBConv block's input tensor in global

memory, thereby producing the layer output with residual shortcut. The inter-block synchronization in the SE layer also ensures that all thread-blocks have read the input tensor before any of them update it with the MBConv output.

The block-fusion kernel computes the full height and width of the activation tensors in each processor, effectively limiting the maximum resolution of the input images. If the height and width are too large, then the blocks of the activation tensors will not fit in local memory. We could extend the basic block-fusion algorithm to partition the activation tensors in the height or width dimensions in addition to the channels dimension and assign different blocks to different processors. This would decrease the amount of local memory used by each processor, but it would also require additional inter-processor communication to exchange the overlapping “halos” of the inputs to the grouped convolution layer. For example, each processor could load an $h \times W \times C$ tile from the input tensor, where $h < H$, and compute the first point-wise convolution for its channel group, yielding an $h \times W \times r$ tensor, where $r < \alpha C$. Then each processor would exchange its top and bottom rows with its neighbor, so that each now has a $(h+2) \times W \times r$ tile of hidden-layer activations. Then each processor computes the grouped convolution, producing an $h \times W \times r$ tile of activations.

The cost of this high-resolution block-fusion kernel is additional global memory buffers, additional global memory data movement for halo exchange, and inter-processor synchronization. However the extra data movement is much less than what is required to load the input activation tensors and store the output activation tensors. We could increase the number of hidden-layer channels computed by each processor and decrease the tile size to keep the local memory allocation constant. This adjustment would increase the arithmetic intensity of the kernel with respect to the global memory system.

The speed of inter-processor communication and synchronization can be relatively fast if processors are organized to support efficient communication with their neighbors. The distributed shared memory in the NVIDIA H100 GPU is one such example [50].

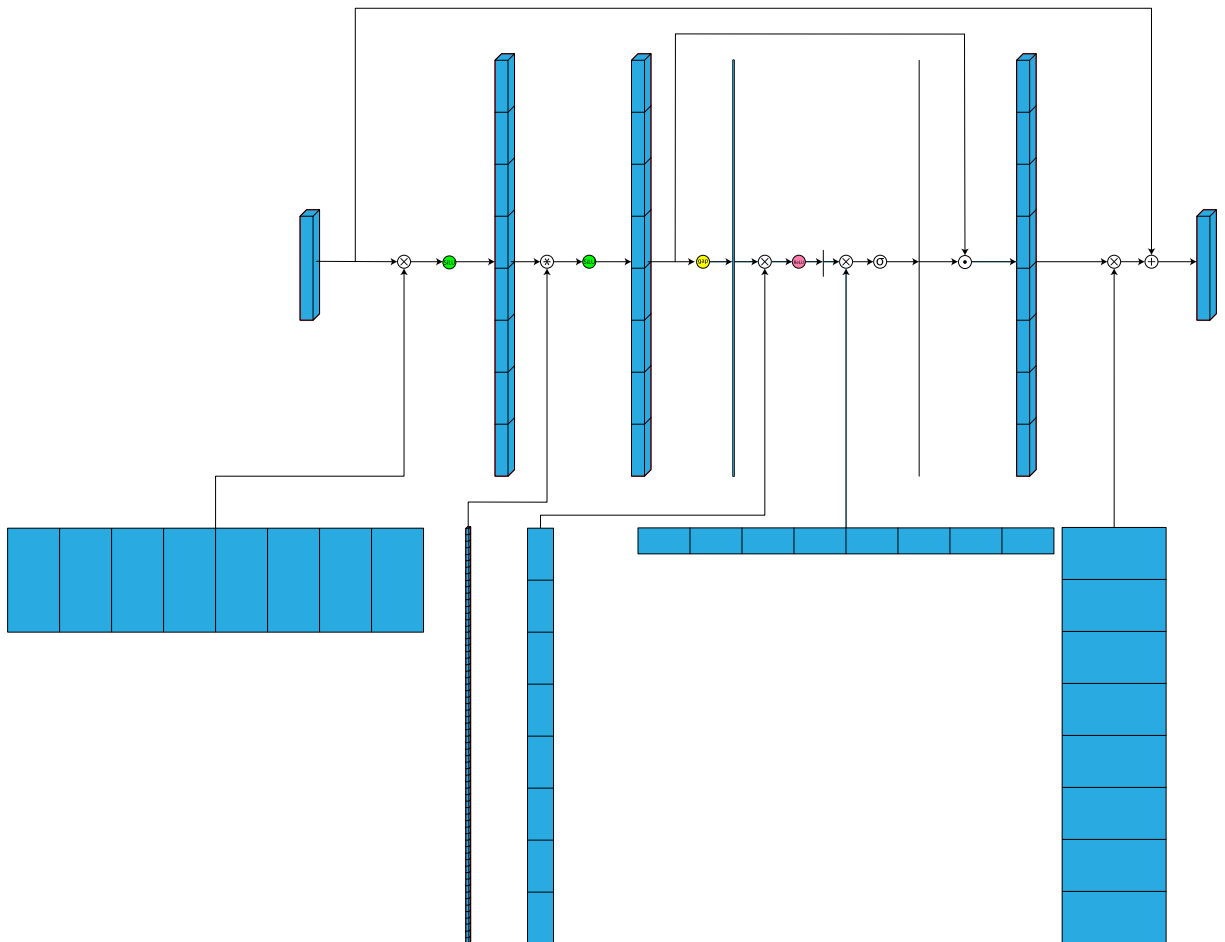


FIGURE 10. Tensor machine for the layer-by-layer execution of MBConv + Squeeze & Excitation. When used in the late stages of a convnet, MBConv blocks have a relatively large number of channels and low-resolution feature maps. The large number of channels causes relatively large operational intensity for the point-wise convolution layers. But the grouped-convolution and SE layers have very low operational intensity, because they perform few operations per activation. We show the weights matrices and activation tensors divided into eight partitions that correspond to the matrix and tensor blocks used by the block-fusion kernel in the next figure.

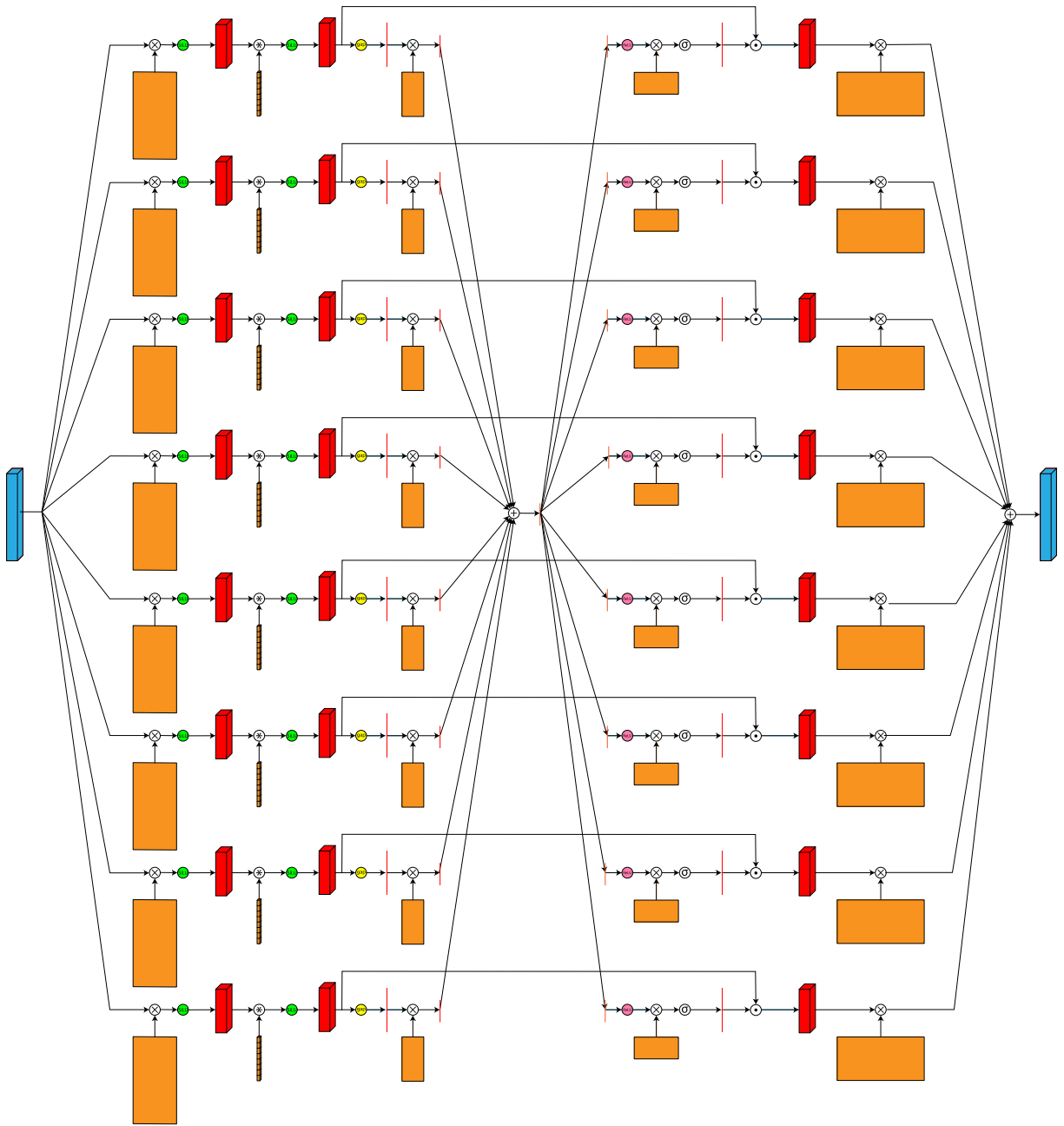


FIGURE 11. Tensor machine for the block-fusion of MBConv + Squeeze & Excitation. Multiple processors compute the MBConv block in parallel, with each processor computing a partition of the hidden-layer channels. The hidden-layer activations never leave the local memory of the processor that computes them. Each processor loads only the weights corresponding to its channels assignment. The “squeeze” operation of the SE layer accumulates the contributions from each processor onto a tensor in global memory. The residual shortcut is implemented by accumulating the output tensor onto the input tensor. The kernel has great operational intensity but uses a lot of global memory bandwidth. When implemented on an NVIDIA GA102 [52], the performance is limited by the latency of inter-processor synchronization. The kernel would be more efficient on the Hopper GPU architecture [50], using distributed shared memory for inter-processor communication.

5.4.2. Waterline Analysis of MBConv

Figure 12 shows the waterline analysis of the MBConv single-layer and block-fusion kernels across a range of block hyperparameters. As mentioned, these kernels were designed for low-resolution feature maps found in the late stages of a convnet, so we use $16_H \times 16_W$ and $8_H \times 8_W$. Late vision blocks also have a relatively large number of channels, so we use $C = 128$ and $C = 256$. We also use bottleneck expansion ratio equal to four.

Point-wise convolution kernels are memory bound with 128 channels and are barely compute bound with 256 channels. The grouped convolution layers are also memory bound, as well as the SE layers.

The block-fusion kernels have very large operational intensity and are strongly compute bound. The minimum attainable latency of the block-fusion kernels is about one half to one third that of layer-by-layer execution.

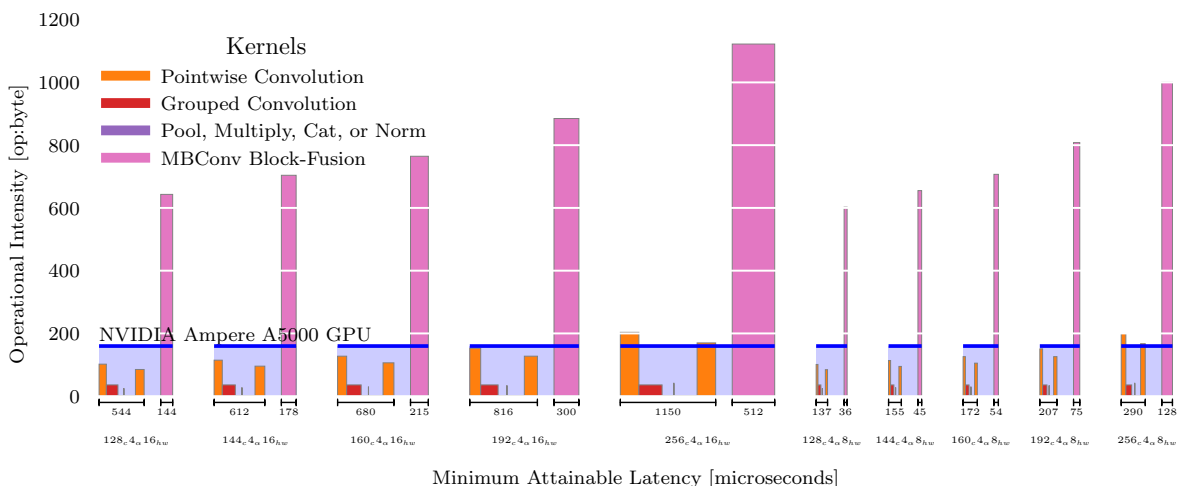


FIGURE 12. Waterline plot for the MBConv block with single-layer and block-fusion kernels. Single-layer kernels are memory-bound for grouped convolution, Squeeze & Excitation layers, and some point-wise convolutions. The block-fusion kernels are strongly compute bound.

5.5. CUDA Kernels

We implemented the ConvFirst and MBConv block-fusion kernels in CUDA [48]. We used code generation to create helper classes to simplify tensor indexing. These classes compute the offset for a given index using named-dimensions. For example, the tensor spec

```
OutputIdx=dict(k8=8, n=128, p=64, q=64, k2=4)
```

generates a CUDA class that can be used like this:

```
st_outputs[OutputIdx().p(thread_p).q(thread_q).k8(k8)] = val;
```

The indexing methods use `constexpr` so that the compiler can simplify the indexing arithmetic at compile time. We found that the use of dimension names when accessing high-dimensional tensors greatly improved the clarity of the source code without sacrificing computational efficiency.

We also used code generation to implement classes that define static kernel parameters, such as tile sizes. This enabled us to enumerate many kernel configurations in Python without adding to the complexity of the CUDA source code.

To launch our block-fusion kernels from Python, we implemented a `Kernel` base class that uses the CuPy [55] package to compile and launch kernels. We implemented an auto-tune method that enumerates all valid kernel configurations for the given block parameters, runs each with random weights and inputs, and selects the fastest.

To integrate our kernels with PyTorch [3], we implemented a `TorchBlock` base class that derives from `torch.nn.Module`. Each `TorchBlock` derived class has a corresponding `Kernel` class. The first call to the `TorchBlock.forward` method calls `Kernel.auto_tune` to select the fastest kernel configuration for the block parameters. The kernel is then stored in the block object and launched using CuPy. We use CuPy to capture a CUDA graph and use the graph in the benchmarks to reduce kernel launch overhead.

This approach gives us a simple way to implement a custom inference backend that runs in PyTorch. In principle, we could run an entire network this way. In this paper, we simply benchmark a stage composed of multiple `ConvFirst` or `MBCConv` blocks.

5.5.1. ConvFirst CUDA Kernel

The `ConvFirst` block-fusion kernel uses thread-blocks with eight warps (i.e., hardware-threads). The kernel computes a $p \times q \times K$ output tile by first loading the corresponding $(p + 2) \times (q + 2) \times C$ input tile into shared local memory (smem), where C and K are the number of input and output channels, and p and q are the height and width of the output tile. The kernel uses `float16` arithmetic with NVIDIA tensor core acceleration.

The warps compute the groups of the convolution layer in parallel, using the NVIDIA `mma.m16n8k8.f16` matrix multiply instruction, which fits the group-width of eight, and store the $p \times q \times C$ output to shared local memory. If $C == K$ and `stride == 1`, the block has a residual shortcut connection, and each warp simultaneously loads a tile of $\frac{p \times q}{8} \times C$

input values from smem and uses them to initialize the registers that accumulate the second linear transformation of the FFN layer. Thus the block input is added to the output during the first iteration of the FFN layer’s multiply-accumulate operations.

More significantly, the residual shortcut does not cause an extra load from the global memory system, as it would in layer-by-layer execution. Instead, the block-fusion kernel loads the shortcut activations from smem, where they were previously stored for the grouped convolution.

Now that the grouped-convolution layer is computed and the FFN accumulators are initialized, we are ready to compute the FFN layer. Each warp loads a $\frac{p \times q}{8} \times C$ tile of the grouped-convolution outputs into registers. Then each warp uses Equation (32) to compute a small number of hidden channels r , convert the `float32` output to `float16`, add bias and apply the ReLU activation function, and reformat the values as input fragments for the `mma.m16n8k8.f16` instruction. Then the fragments are multiplied by the corresponding weights of the second linear transform in the FFN layer with the result accumulated onto the output tile. Note that the hidden-layer activations never leave the register file.

The kernel loops over r hidden channels at a time, asynchronously loading the corresponding columns and rows of the FFN layer weights matrices at each iteration. After the last iteration, the kernel adds the FFN layer’s output bias to the accumulators, converts them from `float32` to `float16`, and stores the result to the output tile in global memory.

Ideally $\frac{p \times q}{8}$ is a multiple of 16 and r is a multiple of 8 so that the hidden activations tile with shape $\frac{p \times q}{8} \times r$ fits the NVIDIA `mma.m16n8k8.f16` or `mma.m16n8k16.f16` matrix multiply instruction. $p \times q$ should be large enough to hide the latency of loading the weights from L2 cache, and $\frac{p \times q}{8}$ should be large enough to hide the latency of loading the weights from smem.

Of course $\frac{p \times q}{8} \times C$ input values of type `float16` and $\frac{p \times q}{8} \times K$ output accumulators of type `float32` must fit in each warp’s registers, in addition to a smaller number of registers for the weights and accumulators of the hidden-layer activations. With a budget of 128 registers per warp, our CUDA kernel performs well with up to 96 channels. This provides sufficient width for the early stages of all but the largest convnets.

The block-fusion and scaling kernel shown in Figure 7(c) would support an arbitrary number of channels, but we did not require it for the networks in this paper.

5.5.2. MBConv CUDA Kernel

We wrote a CUDA kernel that implements the MBConv block. It uses the block-fusion algorithm defined by the tensor machine shown in Figure 11. The kernel uses `float16` arithmetic with NVIDIA tensor core acceleration.

The CUDA kernel uses multiple thread-blocks, assigning a group of 64 hidden-layer channels to each. Each thread-block corresponds to a single processor in Figure 11.

We used atomic adds to implement the additions on buffers in global memory. On NVIDIA GPUs, the global memory is the L2 cache, and atomic counters are used for inter-thread-block synchronization.

Each thread-block computes the full height and width of the activation tensor. Therefore, the kernel computes the convolution layer and global average pooling without any inter-block communication. The maximum resolution that can be supported is limited by the requirement that the $H \times W \times 64_C$ tile of hidden-layer activations must fit in shared local memory. We tested our kernels with $16_H \times 16_W$ and $4_N \times 8_H \times 8_W$ tensors, where N is the batch dimension, so that in both cases the kernel uses 32 KB of shared local memory for activations. This fits easily in the 48 KB of smem available to each thread-block, leaving room for a workspace used for loading weights tensors.

We could support high resolution by assigning spatial partitions of the activation tensor to different thread-blocks. Additional inter-block communication would be needed to compute the convolution and SE layers. It is unclear how much slowdown this extra communication would cause on the Ampere GPU.

Inter-block communication is considerably faster on the next generation Hopper GPU using distributed shared memory. Thread-blocks are organized into clusters that can access each other’s shared memory, enabling inter-block communication that is about $7\times$ faster than global memory [50]. Therefore, the Hopper GPU should make the MBConv kernel more efficient and scalable.

We additionally implemented a *micro-batching* optimization for the MBConv kernel. Given a stage of D consecutive MBConv blocks with feature-map size $H \times W$, we compute the micro-batch size $n < N$ that is required to fully-occupy all 64 streaming multiprocessors on the A5000 GPU. Our kernel computes the first $2n$ images for the first MBConv block in the stage, writing the output to global memory. Then the kernel advances to the next block in the stage, using the $2n$ outputs from the previous block as input. The kernel iterates over $d \leq D$ MBConv blocks before looping back to the first block and processing the next micro-batch of $2n$ images.

The idea is that the $2nHWC$ bottleneck activations of the micro-batch and the ap-

proximately $d(2\alpha C^2 + 72\alpha C)$ weights for the point-wise and grouped-conv2d layers (of the D MBConv blocks with bottleneck expansion ratio α) fit in the L2 cache, so that intermediate activations are not stored to DRAM. Only the input and output to the stack of d blocks are transferred through DRAM. This works because the product HWC is relatively small for the late stages of the convnet where we use MBConv blocks. Micro-batching increases the operational intensity of the MBConv kernel until DRAM memory bandwidth has little impact on kernel performance.

The micro-batch optimization benefits from the fact that the block-fusion kernel does not write hidden-layer activations to global memory, so the number of activations that need to be cached is reduced by a factor of $\alpha + 1$.

5.5.3. Kernel Benchmarks

We benchmarked our kernels in PyTorch using the kernel launch method described in Section 5.5. We used CUDA events to record the start and end time. We skipped 20 iterations of warmup to hide the auto-tune and ensure stability of the GPU clock speed. We timed 100 iterations of the stage execution to get an accurate estimate of the average latency. We benchmarked a stage of eight layers to ensure that weights were not cached between iterations.

We benchmarked PyTorch Inductor by compiling the block module with `torch.compile()` and running with `torch.no_grad()` and `torch.cuda.amp.autocast(dtype=torch.float16)` contexts. We again used warmup iterations to hide any recompilation that might occur on the first iterations.

Our ConvFirst block-fusion kernel runs between 4.5× and 14.2× faster than PyTorch Inductor across a range of block configurations. The speedup is greatest when the block is narrowest, confirming the intuition that the single-layer kernels used by Inductor are memory-bound and become more efficient as the operational intensity of the layers increases.

The computational efficiency of the block-fusion kernel can be as low as 35% when the block is very narrow and the bottleneck expansion ratio is small. However, when the number of channels reaches 32 and the expansion ratio equals 6, the kernel is compute bound, and the computational efficiency equals 66.9%, a 13.2× speedup over Inductor. With 64 channels, our kernel reaches 76.2% computational efficiency.

Our MBConv block-fusion kernel runs between 3.0× and 5.4× as fast as PyTorch Inductor. The computational efficiency reaches 46.2% with 128 channels and 51.4% with 256 channels. Varying the height and width of the activation tensor between 16×16

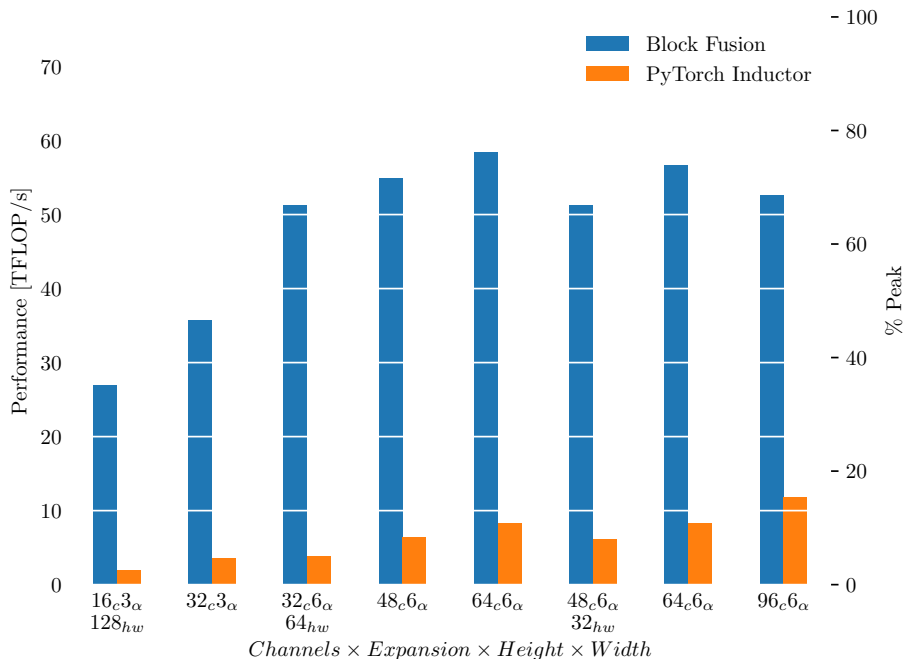


FIGURE 13. ConvFirst block performance in PyTorch, comparing the Inductor backend with our block-fusion kernels. The number of channels C , bottleneck expansion ratio α , and feature map height and width hw were selected from our ConvFirst network, and batch size equals 128. Inductor’s layer-by-layer operation schedule is memory bound, performing poorly when the number of channels is small and improving gradually as the number increases. Our block-fusion algorithm has greater operational intensity and therefore runs 14× faster than Inductor when the number of channels is small and reaches 76% of peak arithmetic throughput with 64 channels.

and 8×8 causes little difference in performance. Performance drops when the number of channels is not a power of two. This is caused by our kernel using a number of thread-blocks that does not evenly divide the GPU’s 64 available SMs.

The MBConv kernel uses very little DRAM bandwidth. Performance is limited by memory latency and the speed of inter-block synchronization. The kernel would be more efficient on a computer that affords fast inter-processor communication, such as the NVIDIA Hopper architecture with distributed shared memory.

TABLE 1. ConvFirst performance with PyTorch-Inductor versus our block-fusion kernels for different numbers of channels, bottleneck expansion ratio (α), and activation tensor size (Height \times Width).

Channels	α	Height	Width	Inductor			Block-Fusion			Speedup
				Time[ms]	TFLOPS	% Peak	Time[ms]	TFLOPS	% Peak	
16	3	128	128	5.88	1.9	2.5	0.42	26.9	35.1	14.2
32	3	128	128	9.89	3.6	4.7	0.99	35.7	46.6	9.9
32	6	64	64	3.94	3.9	5.1	0.30	51.3	66.9	13.2
48	6	64	64	5.06	6.4	8.4	0.59	54.9	71.6	8.6
64	6	64	64	6.75	8.3	10.9	0.96	58.4	76.2	7.0
48	6	32	32	1.33	6.1	8.0	0.16	51.3	67.0	8.4
64	6	32	32	1.70	8.3	10.8	0.25	56.7	74.0	6.8
96	6	32	32	2.60	11.8	15.4	0.58	52.6	68.7	4.5

TABLE 2. MBConv performance with PyTorch-Inductor versus our block-fusion kernels.

Channels	α	Height	Width	SE Ratio	Inductor			Block-Fusion			Speedup
					Time[ms]	TFLOPS	% Peak	Time[ms]	TFLOPS	% Peak	
128	4	16	16	0.25	11.46	7.7	10.0	2.48	35.4	46.2	4.6
144	4	16	16	0.25	13.38	8.1	10.6	3.19	34.0	44.4	4.2
160	4	16	16	0.25	14.81	8.9	11.6	4.09	32.1	41.9	3.6
192	4	16	16	0.25	17.78	10.3	13.5	5.39	34.1	44.4	3.3
256	4	16	16	0.25	24.30	12.9	16.8	8.01	39.1	51.0	3.0
128	4	8	8	0.25	3.43	6.4	8.4	0.64	34.5	45.0	5.4
144	4	8	8	0.25	4.03	6.7	8.8	1.09	25.0	32.5	3.7
160	4	8	8	0.25	4.36	7.5	9.8	1.37	24.0	31.3	3.2
192	4	8	8	0.25	5.18	8.9	11.6	1.39	33.1	43.1	3.7
256	4	8	8	0.25	7.56	10.4	13.5	1.99	39.4	51.4	3.8

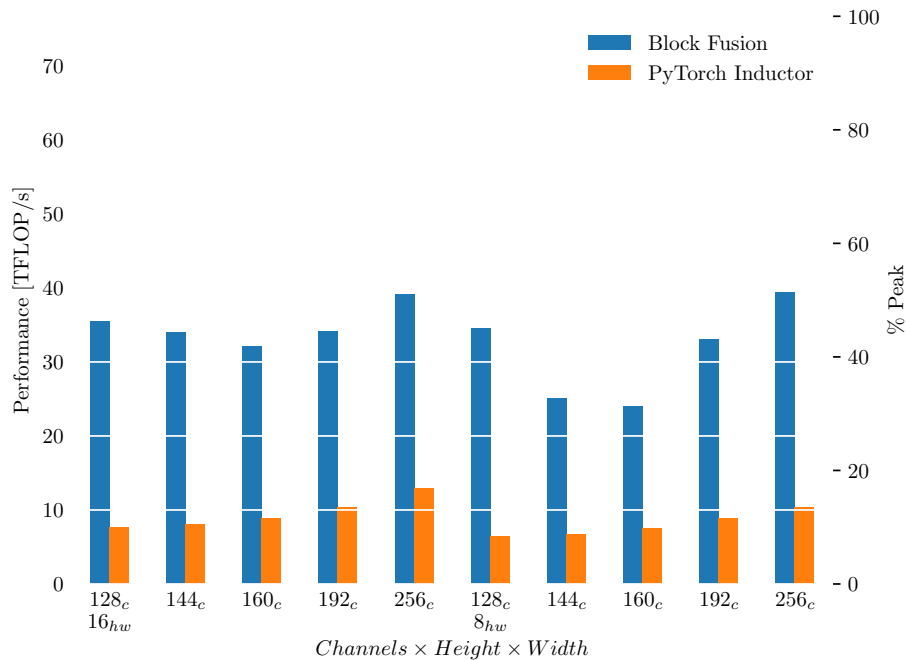


FIGURE 14. MBConv block performance with PyTorch-Inductor versus our block-fusion kernels. We varied the number of channels, height and width over the range of parameters used in our ConvFirst network. Bottleneck expansion ratio equals 4 and batch size equals 128 for all experiments. Inductor’s layer-by-layer execution is severely memory bound for some layers of the MBConv block, while our fused-layer algorithm has large operational intensity. Inter-block synchronization proves costly for our kernels, limiting performance to 51% of peak arithmetic throughput. Our kernels still run 3× to 5.4× faster than Inductor.

5.6. Depth-First Execution

Many papers have pursued the idea of depth-first execution of convnets [1, 19, ...]. The idea is to compute only a small tile of activations in the first layer, then immediately compute all the outputs in the next layer that can be produced from it. By chaining several layers together in this fashion, one can compute several layers at a time while keeping the activation tiles small enough to fit in on-chip memory.

Global operators like Squeeze-and-Excitation prevent depth-first execution. Because every output of these layers depends on every input, there is no depth-first partition of the computational graph. Therefore, depth-first execution cannot be applied to the MBConv+SE blocks used in this paper.

But depth-first execution complements the ConvFirst block-fusion kernels. One would consider a ConvFirst block as a specialized 3×3 convolutional layer with *NHWC* input and output tensors and large arithmetic intensity with respect to its weights. The dependency analysis for partitioning the activation tensors into smaller tiles is the same as for a regular 3×3 convolution. Therefore, we can enjoy the small memory footprint of a depth-first execution across a stack of ConvFirst blocks.

Without block-fusion kernels, the ConvFirst blocks appear as a grouped convolution followed by two point-wise convolutions. Each of these separately has much smaller arithmetic intensity than the block-fusion kernel, so depth-first execution of un-fused layers would require more data movement in the on-chip global memory system. Also it would require additional global memory for storing tiles of the hidden-layer activations. Therefore, we can minimize data movement at all layers of the memory hierarchy by using depth-first execution in conjunction with block-fusion kernels.

Additionally, depth-first execution requires a tile schedule that spans multiple layers with some synchronization between tiles. This might be difficult to map to the CUDA programming model and the large parallelism of GPUs. On the other hand, it could be very efficient on small accelerators where the memory efficiency would prove most beneficial.

6. ConvFirstNet: Striving for Computational Efficiency and Model Efficiency

With the goal of co-optimizing model efficiency and computational efficiency, we used the ConvFirst and MBConv blocks to design a convnet model called ConvFirstNet.

6.1. The Design of ConvFirstNet

We used ConvFirst blocks for the early stages (1-3) and MBConv blocks for the late stages (4-5). This division between light-weight early vision stages and high-capacity late vision stages is inspired by EfficientNetV2 [64]. However, our ConvFirst block uses many fewer operations and parameters than the FusedMBConv block used by EfficientNetV2.

Similar to NFNet [6], ConvFirstNet increases the number of channels between the third and fourth stages by a large factor. Unlike other models, ConvFirstNet uses the same number of blocks in the fourth and fifth stages.

We used group-width equal to eight for all grouped convolutions because it is the smallest width that is divisible by the NVIDIA `mma.m16n8k8.f16` matrix-multiply instruction. In CIFAR experiments, we found group-width equal to four yielded the best model efficiency. Eight and one (depth-wise) both used slightly more operations to achieve the same accuracy. We would prefer group-width four on hardware that computed it efficiently.

We used an expansion ratio equal to three in the bottleneck of the first ConvFirst block to reduce the amount of computation done by this stage. This might have been a mistake, because a larger expansion ratio would increase the operational intensity and yield better computational efficiency. Another interesting idea is to replace the stem and first stage with a *patchify* layer with stride equal to four, as ConvNeXt does.

Stages two and three use ConvFirst with expansion ratio equal to six. This is inspired by the large expansion ratios used by EfficientNet’s bottleneck blocks.

Stages four and five use MBConv with expansion ratio equal to four. We chose this smaller ratio to decrease the number of operations performed by each block, because setting group-width equal to eight increased the number of operations relative to the typical MBConv block with depth-wise convolution.

The MBConv block has a Squeeze & Excitation layer with squeeze-ratio equal to 0.25, same as EfficientNet.

The complete model definitions are listed in Table 3. These architecture hyperparameters worked best across a small range of tested models. The choices are undoubtedly suboptimal and could be improved by a thorough search of the design space. In particular, the ConvFirst-Small model is likely too wide and shallow. Simply increasing the depth of ConvFirstNet-Small might produce an efficient ConvFirstNet-Medium.

All models use the same 256×256 image resolution. The power-of-two size ensures that the activation tensors at every stage are evenly divisible by the matrix fragments used by NVIDIA tensor cores.

6.2. Waterline Analysis of ConvFirstNet

Figure 15 compares the waterline analyses of ConvFirstNet-Small using single-layer and block-fusion kernels. Similar to EfficientNet, ConvFirst-Small is severely memory-bound with layer-by-layer execution. The ConvFirst blocks in the early stages and the grouped convolutions and Squeeze & Excitation layers in the late stages all have very low operational intensity relative to the A5000 op:byte ratio. The resulting maximum computational efficiency equals 36%.

Block-fusion kernels change the picture dramatically. All but the first stage have operational intensity high above the waterline. The resulting maximum computational efficiency equals 97%.

Figure 15 illustrates the peril of using an off-the-shelf inference engine to measure the computational efficiency of a model. Had we used layer-by-layer execution to evaluate the efficiency of ConvFirstNet, we would have judged it to be inferior and discarded it. But ConvFirstNet can attain very high computational efficiency when computed with block-fusion kernels.

Figure 16 shows the effect that increasing op:byte ratio has on maximum attainable efficiency. Block-fusion kernels enable ConvFirst to perform well with relatively little DRAM bandwidth; 80% of peak arithmetic throughput is still attainable when the processor op:byte ratio is 500. Layer-by-layer execution causes both ConvFirst and ConvNeXt to be slow unless the processor has a very low op:byte ratio.

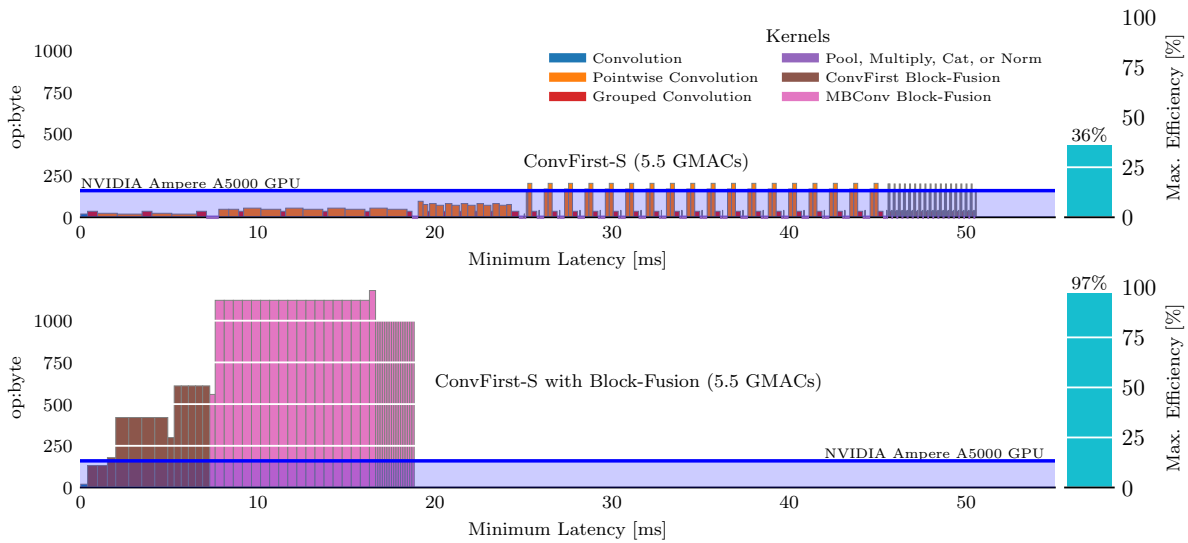


FIGURE 15. Waterline analysis of ConvFirst models. Layer-by-layer execution makes ConvFirst-Net memory bound and severely limits its maximum computational efficiency. Block-fusion kernels make almost the entire network compute bound and near perfect computational efficiency is attainable.

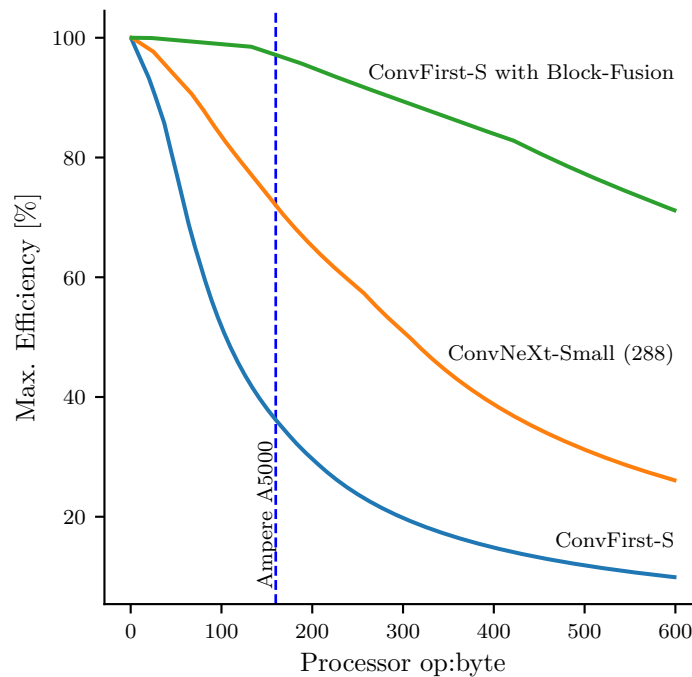


FIGURE 16. Maximum attainable computational efficiency of ConvFirstNet and ConvNeXt over a range of processor op:byte ratios. Block fusion kernels make the networks efficient even when the processor has significantly greater op:byte ratio than our baseline A5000 GPU. Layer-by-layer execution requires very low op:byte ratios for efficient operation.

TABLE 3. ConvFirstNet uses narrow, computationally efficient ConvFirst blocks in the early stages of the network and wide, high capacity MBConv blocks in the late stages. The division between early and late stage vision was inspired by EfficientNetV2. All Conv2d layers use 3×3 kernels. In the ConvFirst and MBConv blocks, the Conv2d layers also use group-width equal to 8, which matches the dimensions of the NVIDIA tensor core `mma.m16n8k8` instruction. The point-wise convolution layers do not use groups. ConvFirst6 is a ConvFirst block with 6 times as many hidden channels as input channels, and MBConv4 is an MBConv block with $4\times$ expansion. MBConv blocks have Squeeze & Excitation layers with squeeze-ratio equal to 0.25. The Conv layer stem and ConvFirst blocks use ReLU activations and MBConv uses SiLU.

ConvFirstNet-Pico				
Stage	Block	Stride	#Channels	#Blocks
0	Conv	2	16	1
1	ConvFirst3	1	16	1
2	ConvFirst6	2	32	2
3	ConvFirst6	2	48	3
4	MBConv4, SE0.25	2	128	11
5	MBConv4, SE0.25	2	128	11
Head	Conv1x1, Pool, FC		1280	1

ConvFirstNet-Nano				
Stage	Block	Stride	#Channels	#Blocks
0	Conv	2	24	1
1	ConvFirst3	1	24	1
2	ConvFirst6	2	48	3
3	ConvFirst6	2	64	4
4	MBConv4, SE0.25	2	160	14
5	MBConv4, SE0.25	2	160	14
Head	Conv1x1, Pool, FC		1280	1

ConvFirstNet-Tiny				
Stage	Block	Stride	#Channels	#Blocks
0	Conv	2	24	1
1	ConvFirst3	1	24	2
2	ConvFirst6	2	48	5
3	ConvFirst6	2	72	6
4	MBConv4, SE0.25	2	192	18
5	MBConv4, SE0.25	2	192	18
Head	Conv1x1, Pool, FC		1280	1

ConvFirstNet-Small				
Stage	Block	Stride	#Channels	#Blocks
0	Conv	2	32	1
1	ConvFirst3	1	32	2
2	ConvFirst6	2	64	5
3	ConvFirst6	2	96	6
4	MBConv4, SE0.25	2	256	18
5	MBConv4, SE0.25	2	256	18
Head	Conv1x1, Pool, FC		1280	1

6.3. ConvFirstNet Model Experiments

We implemented the ConvFirst model in PyTorch [3] and trained it using the PyTorch Image Models framework [70]. We trained for 600 epochs with `float16` precision using `native-amp` and an initial learning rate of 0.128 with 3 epochs of warmup [20]. We used image size equal to 224×224 for training and 256×256 for inference for all model sizes. We trained with eight NVIDIA A6000 GPUs, each with batch size 256, for a total batch size of 2048. Momentum was equal to 0.9 and weight-decay was 1.0e-05. We used the RMSprop optimizer with “TensorFlow style epsilon”, decay epochs equal to 2.4, and decay rate equal to 0.97. These optimizer settings were inspired by EfficientNet. ConvFirst-Pico used dropout equal to 0.2 and the rest used 0.3. All models used drop-path (i.e., stochastic depth [29]) equal to 0.2. We used data augmentation with the auto-augment setting `rand-m9-mstd0.5`, which corresponds to RandAugment [9] with magnitude 9 and noise of standard deviation equal to 0.5. We also used random-erase [77] in “pixel” mode with probability equal to 0.2. We used an exponential moving average of the weights.

We benchmarked the baseline models using the implementations included with PyTorch Image Models and the `benchmark.py` script. We used precision `float16` and `--channels-last`, `--torchcompile=inductor`, `--bench=inference`, and set the batch size equal to 128. We set the GPU and memory clocks to the same values used in the block-fusion benchmarks in the previous section.

We did not implement block-fusion kernels for all the blocks of ConvFirstNet. Specifically, ConvFirst and MBConv with stride 2, ConvFirst with 24 channels, and the stem convolution were not implemented. However the unimplemented layers account for a small fraction of the total network computation, so we can reasonably estimate the performance of the entire network using the measured latency for the implemented blocks and estimates for the rest. See Appendix A for details.

6.4. Results

The speed and accuracy results for ConvFirstNet with block-fusion kernels and baseline models with PyTorch Inductor are listed in Table 4. ConvFirstNet with block-fusion has greater model efficiency than EfficientNet and greater computational efficiency than ConvNeXt with PyTorch Inductor.

Figure 17 shows efficiency gap plots comparing ConvFirstNet and ConvNeXt. ConvFirstNet has a significant model efficiency advantage over ConvNeXt, and the block-fusion kernels make ConvFirstNet more computationally efficient also. The combination

of efficient model and operationally intense algorithms makes ConvFirstNet’s actual latency lower than ConvNeXt’s ideal latency.

TABLE 4. ConvFirstNet Speed and Accuracy. Our ConvFirst model with block-fusion has greater model efficiency than EfficientNet and greater computational efficiency than ConvNeXt. The combined advantages of an efficient model with memory-efficient algorithms gives ConvFirst frame rates (FPS) approximately 4× faster than the baseline at equal accuracy. We measured ImageNet-1K classification accuracy and latency using an NVIDIA Ampere A5000 GPU with 76.7 TFLOP/s peak arithmetic throughput and batch size 128. All models used PyTorch. ConvFirst used our block-fusion kernels and the rest used PyTorch Inductor.

Model	Params [M]	MACs [B]	Latency [ms]	FPS	% Peak	Accuracy [%]
ConvNeXt Femto (288)	5.2	1.3	23.4	5,474.8	18.6	78.7
EfficientNet B1	7.8	0.8	49.9	2,566.8	5.2	79.1
ConvFirst Pico	5.9	0.9	6.1	21,059.6	47.2	79.9
EfficientNet B2	9.1	1.1	66.1	1,935.9	5.7	80.1
ConvNeXt Pico (288)	9.1	2.3	31.7	4,033.3	23.9	80.4
ConvNeXt Nano (288)	15.6	4.1	46.7	2,742.5	29.0	81.5
EfficientNet B3	12.2	2.0	107.5	1,190.4	6.2	81.6
ConvFirst Nano	10.2	1.8	13.5	9,447.2	44.6	81.8
ConvNeXt Tiny	28.6	7.4	80.6	1,587.8	30.6	82.7
ConvFirst Tiny	17.2	3.2	24.1	5,311.0	44.7	82.8
EfficientNet B4	19.3	4.5	203.7	628.3	7.4	82.9
ConvFirst Small	28.6	5.5	33.2	3,851.0	55.2	83.3
EfficientNet B5	30.4	9.6	385.1	332.4	8.3	83.6
ConvNeXt Small (288)	50.2	14.4	138.4	925.1	34.7	83.7
EfficientNetv2 S	21.5	8.4	146.0	876.8	19.3	83.9

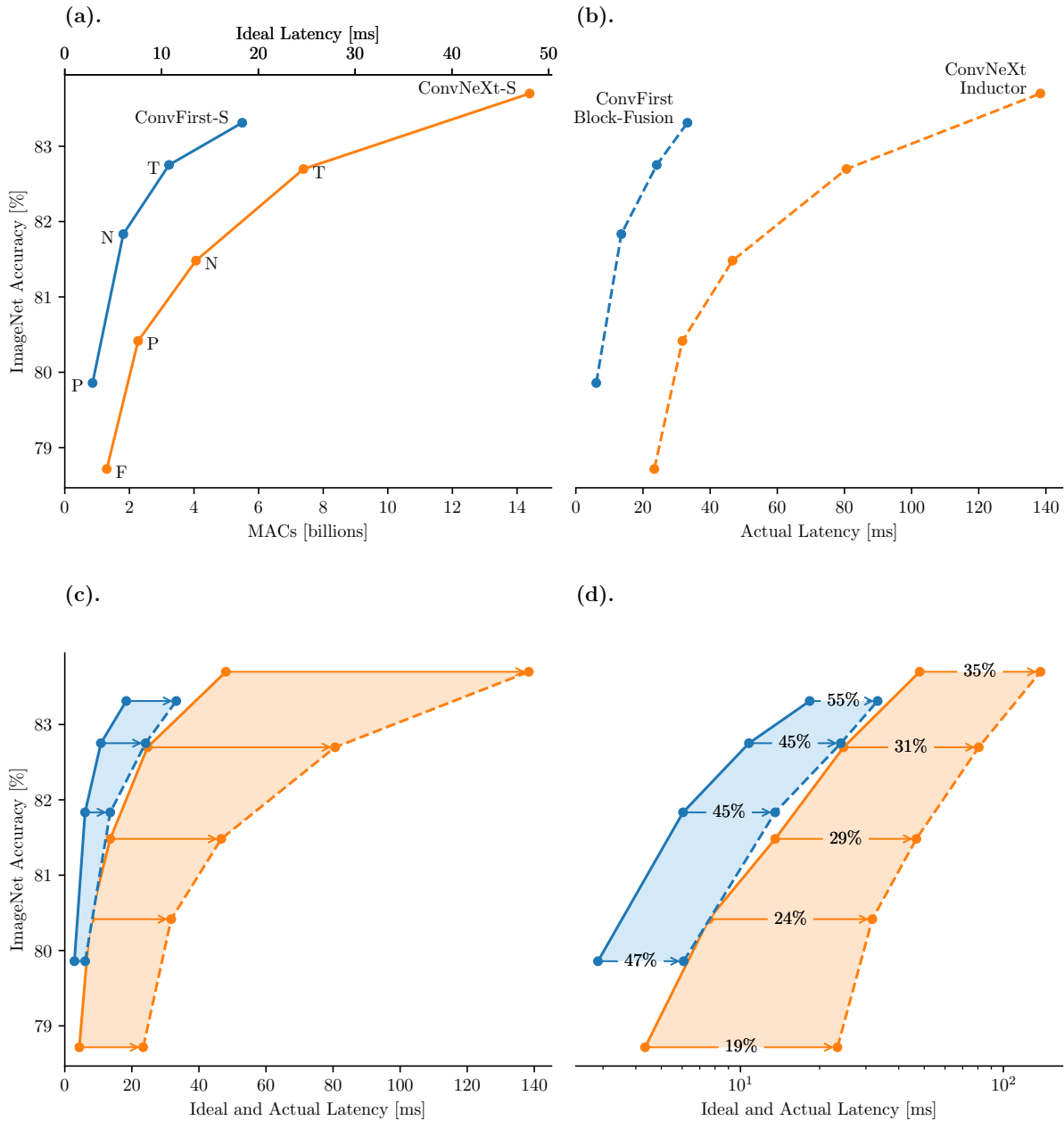


FIGURE 17. ConvFirst with block-fusion versus ConvNeXt with PyTorch Inductor. **(a).** Our ConvFirst model has significantly better model efficiency than ConvNeXt, achieving greater accuracy with fewer operations. **(b).** ConvFirst extends its lead when actual latency is measured with our block-fusion kernels. **(c).** The actual latency of ConvFirst is lower than the ideal latency of ConvNeXt. **(d).** The narrower efficiency gap of ConvFirst results from greater computational efficiency that ranges from 47% – 55%.

7. Conclusion

We presented a new convnet called ConvFirst that has greater model efficiency than EfficientNet and greater computational efficiency than ConvNeXt, when implemented with our block-fusion kernels.

We observed that modern convnets use blocks composed of degenerate conv2d layers that have relatively low operational intensity. Thus the traditional layer-by-layer execution of convnets is memory bound with limited computational efficiency.

We proposed to make the convnet block the target of optimization and designed block-fusion kernels that run significantly faster than single-layer kernels.

We also developed analytical tools to examine model efficiency. We derived the simple formulas that show how model efficiency and computational efficiency combine to produce latency. We created the efficiency gap plot to show model efficiency and latency on the same axes, despite the prevailing view that these concepts are irreconcilable. We created waterline analysis to study the maximum attainable efficiency of a sequence of parallel kernels. We created tensor machines to illustrate the mechanics of block-fusion kernels.

We have shown that large improvements in convnet efficiency can be made by identifying the separate model and computational sources of efficiency and co-optimizing both. We have also shown that the actual performance of efficient models can be severely memory bound when run with layer-by-layer execution. Therefore, it is no longer acceptable for deep learning researchers to estimate the computational efficiency of a model without also studying the efficiency of the algorithms that compute it.

We believe that deep learning must be studied not just as a mathematical modeling problem, but also as a computer science problem. A model's strength is determined not only by the accuracy that it achieves, but also by the computational efficiency that it affords. By co-optimizing models and algorithms, we can develop a new wave of convnets that deliver significantly greater performance.

Acknowledgment

The author would like to thank Hyunggi Cho, CEO & Co-Founder of Phantom AI. This project would not have been possible without his unwavering support.

References

- [1] Manoj Alwani et al. “Fused-layer CNN accelerators”. In: *2016 49th Annual IEEE/ACM International Symposium on Microarchitecture (MICRO)*. IEEE. 2016, pp. 1–12.
- [2] Gene M Amdahl. “Validity of the single processor approach to achieving large scale computing capabilities”. In: *Proceedings of the April 18-20, 1967, spring joint computer conference*. 1967, pp. 483–485.
- [3] Jason Ansel et al. “PyTorch 2: Faster Machine Learning Through Dynamic Python Bytecode Transformation and Graph Compilation”. In: (2024).
- [4] Tom M Apostol. *Calculus, Volume 2*. John Wiley & Sons, 1969. ISBN: 0471000078.
- [5] “Backpropagation applied to handwritten zip code recognition”. In: *Neural computation* 1.4 (1989), pp. 541–551.
- [6] Andy Brock et al. “High-performance large-scale image recognition without normalization”. In: *International Conference on Machine Learning*. PMLR. 2021, pp. 1059–1071.
- [7] François Chollet. “Xception: Deep learning with depthwise separable convolutions”. In: *Proceedings of the IEEE conference on computer vision and pattern recognition*. 2017, pp. 1251–1258.
- [8] Jason Cong and Bingjun Xiao. “Minimizing computation in convolutional neural networks”. In: *International conference on artificial neural networks*. Springer. 2014, pp. 281–290.
- [9] Ekin D Cubuk et al. “Randaugment: Practical automated data augmentation with a reduced search space”. In: *Proceedings of the IEEE/CVF conference on computer vision and pattern recognition workshops*. 2020, pp. 702–703.
- [10] Zihang Dai et al. “Coatnet: Marrying convolution and attention for all data sizes”. In: *Advances in neural information processing systems* 34 (2021), pp. 3965–3977.
- [11] Mostafa Dehghani et al. “Scaling vision transformers to 22 billion parameters”. In: *International Conference on Machine Learning*. PMLR. 2023, pp. 7480–7512.
- [12] Mostafa Dehghani et al. “The efficiency misnomer”. In: *arXiv preprint arXiv:2110.12894* (2021).
- [13] Jia Deng et al. “Imagenet: A large-scale hierarchical image database”. In: *2009 IEEE conference on computer vision and pattern recognition*. Ieee. 2009, pp. 248–255.

- [14] Piotr Dollár, Mannat Singh, and Ross Girshick. “Fast and accurate model scaling”. In: *Proceedings of the IEEE/CVF Conference on Computer Vision and Pattern Recognition*. 2021, pp. 924–932.
- [15] Alexey Dosovitskiy et al. “An image is worth 16x16 words: Transformers for image recognition at scale”. In: *arXiv preprint arXiv:2010.11929* (2020).
- [16] Stefan Elfving, Eiji Uchibe, and Kenji Doya. “Sigmoid-weighted linear units for neural network function approximation in reinforcement learning”. In: *Neural networks* 107 (2018), pp. 3–11.
- [17] Johannes de Fine Licht et al. “StencilFlow: Mapping large stencil programs to distributed spatial computing systems”. In: *2021 IEEE/ACM International Symposium on Code Generation and Optimization (CGO)*. IEEE. 2021, pp. 315–326.
- [18] DH Fowler. “An approximation technique, and its use by Wallis and Taylor”. In: *Archive for history of exact sciences* (1991), pp. 189–233.
- [19] Koen Goetschalckx and Marian Verhelst. “Breaking high-resolution CNN bandwidth barriers with enhanced depth-first execution”. In: *IEEE Journal on Emerging and Selected Topics in Circuits and Systems* 9.2 (2019), pp. 323–331.
- [20] Priya Goyal et al. “Accurate, large minibatch sgd: Training imagenet in 1 hour”. In: *arXiv preprint arXiv:1706.02677* (2017).
- [21] Suyog Gupta and Mingxing Tan. *EfficientNet-EdgeTPU: Creating Accelerator-Optimized Neural Networks with AutoML*. <https://blog.research.google/2019/08/efficientnet-edgetpu-creating.html>. 2019.
- [22] Scott B Guthery. *A motif of mathematics*. Docent Press, 2011.
- [23] Richard HR Hahnloser et al. “Digital selection and analogue amplification coexist in a cortex-inspired silicon circuit”. In: *nature* 405.6789 (2000), pp. 947–951.
- [24] Kaiming He et al. “Deep residual learning for image recognition”. In: *Proceedings of the IEEE conference on computer vision and pattern recognition*. 2016, pp. 770–778.
- [25] Mark D Hill and Alan Jay Smith. “Evaluating associativity in CPU caches”. In: *IEEE Transactions on Computers* 38.12 (1989), pp. 1612–1630.
- [26] Andrew Howard et al. “Searching for mobilenetv3”. In: *Proceedings of the IEEE/CVF international conference on computer vision*. 2019, pp. 1314–1324.
- [27] Andrew G Howard et al. “Mobilenets: Efficient convolutional neural networks for mobile vision applications”. In: *arXiv preprint arXiv:1704.04861* (2017).

- [28] Jie Hu, Li Shen, and Gang Sun. “Squeeze-and-excitation networks”. In: *Proceedings of the IEEE conference on computer vision and pattern recognition*. 2018, pp. 7132–7141.
- [29] Gao Huang et al. “Deep networks with stochastic depth”. In: *Computer Vision–ECCV 2016: 14th European Conference, Amsterdam, The Netherlands, October 11–14, 2016, Proceedings, Part IV 14*. Springer. 2016, pp. 646–661.
- [30] Sergey Ioffe and Christian Szegedy. “Batch normalization: Accelerating deep network training by reducing internal covariate shift”. In: *International conference on machine learning*. pmlr. 2015, pp. 448–456.
- [31] Kevin Jarrett et al. “What is the best multi-stage architecture for object recognition?” In: *2009 IEEE 12th international conference on computer vision*. IEEE. 2009, pp. 2146–2153.
- [32] Norman P Jouppi et al. “In-datacenter performance analysis of a tensor processing unit”. In: *Proceedings of the 44th annual international symposium on computer architecture*. 2017, pp. 1–12.
- [33] Norman P Jouppi et al. “Ten lessons from three generations shaped google’s tpuv4i: Industrial product”. In: *2021 ACM/IEEE 48th Annual International Symposium on Computer Architecture (ISCA)*. IEEE. 2021, pp. 1–14.
- [34] W.T.B. Kelvin. *Popular Lectures and Addresses*. Nature series v. 1. Macmillan and Company, 1889. ISBN: 9780598775993. URL: <https://books.google.com/books?id=MInJzB0gXygC>.
- [35] Ken Kennedy and John R Allen. *Optimizing compilers for modern architectures: a dependence-based approach*. Morgan Kaufmann Publishers Inc., 2001.
- [36] Tamara G Kolda and Brett W Bader. “Tensor decompositions and applications”. In: *SIAM review* 51.3 (2009), pp. 455–500.
- [37] Alex Krizhevsky, Ilya Sutskever, and Geoffrey E Hinton. “Imagenet classification with deep convolutional neural networks”. In: *Advances in neural information processing systems* 25 (2012).
- [38] Andrew Lavin. *Anatomy of a High-Performance MBConv Block*. <https://www.linkedin.com/pulse/anatomy-high-performance-mbconv-block-andrew-lavin>. 2023.
- [39] Andrew Lavin. “maxdnn: An efficient convolution kernel for deep learning with maxwell gpus”. In: *arXiv preprint arXiv:1501.06633* (2015).

- [40] Andrew Lavin. *Phantom Inference Engine (PiE): A Software Approach to Faster Neural Networks*. <https://www.linkedin.com/pulse/phantom-inference-engine-pie-software-approach-faster-andrew-lavin>. 2021.
- [41] Andrew Lavin and Scott Gray. “Fast algorithms for convolutional neural networks”. In: *Proceedings of the IEEE conference on computer vision and pattern recognition*. 2016, pp. 4013–4021.
- [42] Yann LeCun et al. “Gradient-based learning applied to document recognition”. In: *Proceedings of the IEEE* 86.11 (1998), pp. 2278–2324.
- [43] Sheng Li et al. “Searching for fast model families on datacenter accelerators”. In: *Proceedings of the IEEE/CVF Conference on Computer Vision and Pattern Recognition*. 2021, pp. 8085–8095.
- [44] Min Lin, Qiang Chen, and Shuicheng Yan. “Network in network”. In: *arXiv preprint arXiv:1312.4400* (2013).
- [45] Ze Liu et al. “Swin transformer: Hierarchical vision transformer using shifted windows”. In: *Proceedings of the IEEE/CVF international conference on computer vision*. 2021, pp. 10012–10022.
- [46] Zhuang Liu et al. “A convnet for the 2020s”. In: *Proceedings of the IEEE/CVF conference on computer vision and pattern recognition*. 2022, pp. 11976–11986.
- [47] Michael Mathieu, Mikael Henaff, and Yann LeCun. “Fast training of convolutional networks through ffts”. In: *arXiv preprint arXiv:1312.5851* (2013).
- [48] NVIDIA. *CUDA C++ Programming Guide*. <https://docs.nvidia.com/cuda/cuda-c-programming-guide/index.html>.
- [49] NVIDIA. *GPU Performance Background User’s Guide*. <https://docs.nvidia.com/deeplearning/performance/dl-performance-gpu-background/index.html>. Accessed on February 3, 2024.
- [50] NVIDIA. *H100 tensor core GPU architecture overview*. <https://resources.nvidia.com/en-us-tensor-core/gtc22-whitepaper-hopper>. 2022.
- [51] NVIDIA. *Matrix Multiplication Background User’s Guide*. <https://docs.nvidia.com/deeplearning/performance/dl-performance-matrix-multiplication/index.html>. Accessed on February 3, 2024.
- [52] NVIDIA. *NVIDIA AMPERE GA102 GPU ARCHITECTURE*. <https://www.nvidia.com/content/PDF/nvidia-ampere-ga-102-gpu-architecture-whitepaper-v2.pdf>. 2022.

- [53] NVIDIA. *NVIDIA TESLA V100 GPU ARCHITECTURE*. <https://images.nvidia.com/content/volta-architecture/pdf/volta-architecture-whitepaper.pdf>. 2017.
- [54] NVIDIA. *Parallel Thread Execution ISA Version 8.4*. <https://docs.nvidia.com/cuda/parallel-thread-execution/>. 2024.
- [55] Ryosuke Okuta et al. “CuPy: A NumPy-Compatible Library for NVIDIA GPU Calculations”. In: *Proceedings of Workshop on Machine Learning Systems (LearningSys) in The Thirty-first Annual Conference on Neural Information Processing Systems (NIPS)*. 2017. URL: http://learningsys.org/nips17/assets/papers/paper_16.pdf.
- [56] Ilija Radosavovic et al. “Designing network design spaces”. In: *Proceedings of the IEEE/CVF conference on computer vision and pattern recognition*. 2020, pp. 10428–10436.
- [57] Jonathan Ragan-Kelley et al. “Halide: a language and compiler for optimizing parallelism, locality, and recomputation in image processing pipelines”. In: *Acm Sigplan Notices* 48.6 (2013), pp. 519–530.
- [58] Prajit Ramachandran, Barret Zoph, and Quoc V Le. “Searching for activation functions”. In: *arXiv preprint arXiv:1710.05941* (2017).
- [59] Mark Sandler et al. “Mobilenetv2: Inverted residuals and linear bottlenecks”. In: *Proceedings of the IEEE conference on computer vision and pattern recognition*. 2018, pp. 4510–4520.
- [60] Pierre Sermanet et al. “Overfeat: Integrated recognition, localization and detection using convolutional networks”. In: *arXiv preprint arXiv:1312.6229* (2013).
- [61] Karen Simonyan and Andrew Zisserman. “Very deep convolutional networks for large-scale image recognition”. In: *arXiv preprint arXiv:1409.1556* (2014).
- [62] Samuel L Smith et al. “Convnets match vision transformers at scale”. In: *arXiv preprint arXiv:2310.16764* (2023).
- [63] Mingxing Tan and Quoc Le. “Efficientnet: Rethinking model scaling for convolutional neural networks”. In: *International conference on machine learning*. PMLR. 2019, pp. 6105–6114.
- [64] Mingxing Tan and Quoc Le. “Efficientnetv2: Smaller models and faster training”. In: *International conference on machine learning*. PMLR. 2021, pp. 10096–10106.

- [65] Mingxing Tan et al. “Mnasnet: Platform-aware neural architecture search for mobile”. In: *Proceedings of the IEEE/CVF conference on computer vision and pattern recognition*. 2019, pp. 2820–2828.
- [66] Ilya O Tolstikhin et al. “Mlp-mixer: An all-mlp architecture for vision”. In: *Advances in neural information processing systems* 34 (2021), pp. 24261–24272.
- [67] Zhengzhong Tu et al. “Maxvit: Multi-axis vision transformer”. In: *European conference on computer vision*. Springer. 2022, pp. 459–479.
- [68] Nicolas Vasilache et al. “Fast convolutional nets with fbfft: A GPU performance evaluation”. In: *arXiv preprint arXiv:1412.7580* (2014).
- [69] Ashish Vaswani et al. “Attention is all you need”. In: *Advances in neural information processing systems* 30 (2017).
- [70] Ross Wightman. *PyTorch Image Models*. <https://github.com/rwightman/pytorch-image-models>. 2019. DOI: 10.5281/zenodo.4414861.
- [71] Ross Wightman, Hugo Touvron, and Hervé Jégou. “Resnet strikes back: An improved training procedure in timm”. In: *arXiv preprint arXiv:2110.00476* (2021).
- [72] Samuel Williams, Andrew Waterman, and David Patterson. “Roofline: an insightful visual performance model for multicore architectures”. In: *Communications of the ACM* 52.4 (2009), pp. 65–76.
- [73] Saining Xie et al. “Aggregated residual transformations for deep neural networks”. In: *Proceedings of the IEEE conference on computer vision and pattern recognition*. 2017, pp. 1492–1500.
- [74] Xuan Yang et al. “Interstellar: Using halide’s scheduling language to analyze dnn accelerators”. In: *Proceedings of the Twenty-Fifth International Conference on Architectural Support for Programming Languages and Operating Systems*. 2020, pp. 369–383.
- [75] Dan Zhang et al. “A full-stack search technique for domain optimized deep learning accelerators”. In: *Proceedings of the 27th ACM International Conference on Architectural Support for Programming Languages and Operating Systems*. 2022, pp. 27–42.
- [76] Richard Zhang. “Making convolutional networks shift-invariant again”. In: *International conference on machine learning*. PMLR. 2019, pp. 7324–7334.
- [77] Zhun Zhong et al. “Random erasing data augmentation”. In: *Proceedings of the AAAI conference on artificial intelligence*. Vol. 34. 07. 2020, pp. 13001–13008.

A. ConvFirstNet Speed Projections

We did not implement all the ConvFirst and MBConv kernels that are required to run ConvFirstNet. The stride-2 kernels, ConvFirst with channels equal to 24, and the stem kernels are not implemented. Therefore, we estimate the network inference time by using the benchmark results of the implemented blocks and efficiency estimates of the unimplemented blocks. We estimate that the stride-2 blocks will run at 80% of the efficiency of the stride-1 blocks, that the ConvFirst block with 24 channels and expansion factor 3 will run at 40% computational efficiency, and the stem convolution will run at 75%.

The stem has 3 input channels and 16, 24, or 32 output channels. It would be fused with the kernel of the first ConvFirst block, significantly reducing the size of the block's input tensor, likely causing the block to run faster. We feel this justifies the relatively high efficiency estimate for the stem.

The unimplemented kernels are a relatively small fraction of the total network, so inaccurate estimates will not greatly affect the accuracy of the network run time projection.

The following tables contain the details of the ConvFirst speed projections.

TABLE 5. ConvFirstNet-Pico speed projection.

Block	N	s	H	W	Ks	K	R	C	t	gw	Ks	K	Conv	Exp	Layer OPs [millions]			Total	% Peak	Est. %Peak	Latency [ms]	TFLOP/s
															Prij	Sqz Exc	Depth					
Stem	128	2	256	256	3	16		3					14.16			1	14.16		75.0%	0.031	57.5	
ConvFirst	128	1	128	128	3	16	48	16	3	8	3	16	37.75	25.17	25.17	1	88.08	35.1%	53.5%	0.419	26.9	
ConvFirst	128	2	128	128	3	16	96	32	6	8	6	16	37.75	25.17	25.17	1	88.08	66.9%	53.5%	0.275	41.0	
ConvFirst	128	1	64	64	3	32	192	32	6	8	6	32	18.87	50.33	50.33	1	119.54		53.6%	0.298	51.3	
ConvFirst	128	2	64	64	3	32	192	48	6	8	6	32	18.87	25.17	18.87	1	62.91		53.6%	0.196	41.1	
ConvFirst	128	1	32	32	3	48	288	48	6	8	6	48	7.08	28.31	28.31	2	127.40	67.0%	37.0%	0.317	51.4	
MBCConv	128	2	32	32	3	128	192	128	4	8	4	48	28.31	18.87	12.58	1	59.78		37.0%	0.270	28.3	
MBCConv	128	1	16	16	3	128	512	128	4	8	4	128	18.87	33.55	33.55	10	860.49	46.2%	36.0%	3.108	35.4	
MBCConv	128	2	16	16	3	128	512	128	4	8	4	128	18.87	33.55	8.39	1	60.88		36.0%	0.282	27.6	
MBCConv	128	1	8	8	3	128	512	128	4	8	4	128	4.72	8.39	8.39	10	215.61	45.0%		0.800	34.5	
Total																	1,696.93		47.2	5.996	36.2	

TABLE 6. ConvFirstNet-Nano speed projection.

Block	N	s	H	W	Ks	K	R	C	t	C	R	K	Conv	Exp	Layer OPs [millions]			Total	% Peak	Est. %Peak	Latency [ms]	TFLOP/s	
															Pj	Sqz	Exc						Depth
Stem	128	2	256	256	3	24	24	3	3	3	24	24	21.23										
ConvFirst	128	1	128	128	3	24	72	24	3	8	24	24	56.62	56.62	56.62	56.62	56.62	56.62	56.62	56.62	56.62	56.62	56.62
ConvFirst	128	2	128	128	3	24	144	48	6	8	24	48	56.62	56.62	56.62	56.62	56.62	56.62	56.62	56.62	56.62	56.62	56.62
ConvFirst	128	1	64	64	3	48	288	48	6	8	48	288	28.31	113.25	113.25	113.25	113.25	113.25	113.25	113.25	113.25	113.25	113.25
ConvFirst	128	2	64	64	3	48	288	64	6	8	48	288	28.31	56.62	56.62	56.62	56.62	56.62	56.62	56.62	56.62	56.62	56.62
ConvFirst	128	1	32	32	3	64	384	64	6	8	64	384	9.44	50.33	50.33	50.33	50.33	50.33	50.33	50.33	50.33	50.33	50.33
MBCConv	128	2	32	32	3	64	256	160	4	8	64	256	37.75	33.55	20.97	0.02	0.02	0.02	0.02	0.02	0.02	0.02	0.02
MBCConv	128	1	16	16	3	160	640	160	4	8	160	640	23.59	52.43	52.43	0.10	0.10	0.10	0.10	0.10	0.10	0.10	0.10
MBCConv	128	2	16	16	3	160	640	160	4	8	160	640	23.59	52.43	52.43	0.10	0.10	0.10	0.10	0.10	0.10	0.10	0.10
MBCConv	128	1	8	8	3	160	640	160	4	8	160	640	5.90	13.11	13.11	0.10	0.10	0.10	0.10	0.10	0.10	0.10	0.10
Total														3,595.07	44.6%		13.441	34.2					

TABLE 7. ConvFirstNet-Tiny speed projection.

Block	N	s	H	W	Ks	gw	t	C	R	K	Conv	Exp	Layer OPs [millions]			Depth	Total	% Peak	Est. %Peak	Latency [ms]	TFLOP/s
													Pj	Sqz	Exc						
Stem	128	2	256	256	3	0	0	3	0	24	21.23	0.00	0.00	0.00	1	21.23	0.0%	75.0%	0.047	57.5	
ConvFirst	128	1	128	128	3	8	3	24	72	24	56.62	56.62	56.62	0.00	2	339.74	0.0%	40.0%	1.417	30.7	
ConvFirst	128	2	128	128	3	8	6	24	144	48	56.62	56.62	56.62	0.00	1	169.87	0.0%	57.3%	0.495	43.9	
ConvFirst	128	1	64	64	3	8	6	48	288	48	28.31	113.25	113.25	0.00	4	1,019.22	71.6%	0.0%	2.376	54.9	
ConvFirst	128	2	64	64	3	8	6	48	288	72	28.31	56.62	42.47	0.00	1	127.40	0.0%	56.0%	0.380	43.0	
ConvFirst	128	1	32	32	3	8	6	72	432	72	10.62	63.70	63.70	0.00	5	690.09	0.0%	70.0%	1.645	53.7	
MBConv	128	2	32	32	3	8	4	72	288	192	42.47	42.47	28.31	0.02	1	113.27	0.0%	33.5%	0.564	25.7	
MBConv	128	1	16	16	3	8	4	192	768	192	28.31	75.50	75.50	0.15	17	3,050.72	41.9%	0.0%	12.151	32.1	
MBConv	128	2	16	16	3	8	4	192	768	192	28.31	75.50	18.87	0.15	1	122.83	0.0%	25.0%	0.819	19.2	
MBConv	128	1	8	8	3	8	4	192	768	192	7.08	18.87	18.87	0.15	17	764.56	31.3%	0.0%	4.076	24.0	
Total																6,418.93	44.7%		23.970	34.3	

TABLE 8. ConvFirstNet-Small speed projection.

Block	N	s	H	W	Ks	gw	t	C	R	K	Conv	Exp	Layer OPs [millions]			Total	% Peak	Est. %Peak	Latency [ms]	TFLOP/s
													Prij	Sqz Exc	Depth					
Stem	128	2	256	256	3	0	0	3	0	32	28.31	0.00	0.00	1	28.31	0.0%	75.0%	0.063	57.5	
ConvFirst	128	1	128	128	3	8	3	32	96	32	75.50	100.66	100.66	2	553.65	46.6%	0.0%	1.983	35.7	
ConvFirst	128	2	128	128	3	8	6	32	192	64	75.50	100.66	100.66	1	276.82	0.0%	61.0%	0.758	46.8	
ConvFirst	128	1	64	64	3	8	6	64	384	64	37.75	201.33	201.33	4	1,761.61	76.2%	0.0%	3.858	58.4	
ConvFirst	128	2	64	64	3	8	6	64	384	96	37.75	100.66	75.50	1	213.91	0.0%	55.0%	0.650	42.2	
ConvFirst	128	1	32	32	3	8	6	96	576	96	14.16	113.25	113.25	5	1,203.24	68.7%	0.0%	2.923	52.7	
MBConv	128	2	32	32	3	8	4	96	384	256	56.62	75.50	50.33	1	182.49	0.0%	40.8%	0.746	31.3	
MBConv	128	1	16	16	3	8	4	256	1024	256	37.75	134.22	134.22	17	5,209.59	51.0%	0.0%	17.047	39.1	
MBConv	128	2	16	16	3	8	4	256	1024	256	37.75	134.22	33.55	1	205.78	0.0%	41.1%	0.835	31.5	
MBConv	128	1	8	8	3	8	4	256	1024	256	9.44	33.55	33.55	17	1,305.74	51.4%	0.0%	4.239	39.4	
Total															10,941.14	55.2%		33.102	42.3	

TABLE 9. ConvFirstNet speed projection. For each of the network sizes, we copy the estimates for the arithmetic utilization (i.e., % Peak) and performance (TFLOP/s) from the previous tables and use it to estimate the latency of the whole network’s latency by dividing MACs by (half) of TFLOP/s. This estimate assumes that the layers left out of the previous tables, namely the layers of the classifier head, have the same average performance as the rest of the network. The head is small compared to the rest of the network, and the bulk of it is a point-wise convolution with a large channel count, which likely could be performed more efficiently than the rest of the network. Therefore, we are likely underestimating network speed slightly by assuming the classifier head runs at the same speed as the rest of the network.

Model	Pars[M]	MACs[B]	Top1[%]	Input Size	Batch	Batch MACs[B]	Device TFLOP/s	% Peak	TFLOP/s	Batch Time[ms]	FPS
ConvFirst-P	5.91	0.86	79.858	256	128	110.1	76.7	47.23%	36.2	6.078	21,060.03
ConvFirst-N	10.17	1.812	81.834	256	128	231.9	76.7	44.64%	34.2	13.549	9,446.95
ConvFirst-T	17.24	3.227	82.752	256	128	413.1	76.7	44.69%	34.3	24.101	5,311.04
ConvFirst-S	28.55	5.493	83.312	256	128	703.1	76.7	55.16%	42.3	33.238	3,851.04

B. Amdahl's Roofline

How much can we improve the minimum attainable latency of a sequence of parallel kernels by reducing the DRAM transfers of a single kernel?

As in Section 4, \mathcal{R} is the peak arithmetic throughput, \mathcal{B} is the peak DRAM memory bandwidth, n_i and b_i are the number of operations and bytes transferred by kernel i , and $\frac{n_i}{b_i}$ is its operational intensity.

If kernel j is memory-bound, then $\frac{n_j}{b_j} < \frac{\mathcal{R}}{\mathcal{B}}$, and its minimum latency is $t_j = \frac{b_j}{\mathcal{B}}$. By reducing the bytes transferred to $\hat{b}_j = \frac{n_j}{\frac{\mathcal{R}}{\mathcal{B}}}$ or less, the kernel becomes compute bound with new minimum latency $\hat{t}_j = \frac{n_j}{\mathcal{R}}$. Therefore, the maximum improvement equals

$$\begin{aligned}
 \frac{T}{\hat{T}} &= \frac{T}{T - t_j + \hat{t}_j} \\
 (33) \quad &= \frac{1}{1 - \frac{t_j}{T} + \frac{\hat{t}_j}{T}} \\
 &= \frac{1}{1 - f_B + f_R}
 \end{aligned}$$

where

$$f_B = \frac{b_j}{\mathcal{B}T}, \quad f_R = \frac{n_j}{\mathcal{R}T}$$

are the minimum latency of the memory bound and compute bound versions of kernel j , measured as a fraction of the total minimum attainable latency before optimization,

$$T = \sum_i t_i.$$

Equation (33) can be understood as a variation of Amdahl's law [2] applied to roofline analysis [72].

If kernel j is already compute bound, then further reducing its DRAM transfers has no effect on minimum latency. Yet it does increase the median operational intensity (Equation 29). This is the reason why the roofline performance model is not correct for a sequence of kernels.